

# GRANOLA: Adaptive Normalization for Graph Neural Networks

Moshe Eliasof <sup>\*1</sup> Beatrice Bevilacqua <sup>\*2</sup> Carola-Bibiane Schönlieb <sup>1</sup> Haggai Maron <sup>3</sup>

## Abstract

In recent years, significant efforts have been made to refine the design of Graph Neural Network (GNN) layers, aiming to overcome diverse challenges, such as limited expressive power and oversmoothing. Despite their widespread adoption, the incorporation of off-the-shelf normalization layers like BatchNorm or InstanceNorm within a GNN architecture may not effectively capture the unique characteristics of graph-structured data, potentially reducing the expressive power of the overall architecture. Moreover, existing graph-specific normalization layers often struggle to offer substantial and consistent benefits. In this paper, we propose GRANOLA, a novel graph-adaptive normalization layer. Unlike existing normalization layers, GRANOLA normalizes node features by adapting to the specific characteristics of the graph, particularly by generating expressive representations of its neighborhood structure, obtained by leveraging the propagation of Random Node Features (RNF) in the graph. We present theoretical results that support our design choices. Our extensive empirical evaluation of various graph benchmarks underscores the superior performance of GRANOLA over existing normalization techniques. Furthermore, GRANOLA emerges as the top-performing method among all baselines within the same time complexity of Message Passing Neural Networks (MPNNs).

## 1. Introduction

Graph Neural Networks (GNNs) have achieved remarkable success in several application domains, ranging from bioinformatics (Jumper et al., 2021) to Computer Vision (Wang et al., 2019), showcasing their ability to leverage the rich structural information within graph data. Recently, a

<sup>\*</sup>Equal contribution <sup>1</sup>Department of Applied Mathematics and Theoretical Physics, University of Cambridge, UK. <sup>2</sup>Department of Computer Science, Purdue University, USA. <sup>3</sup>Department of Electrical Engineering, Technion - Israel Institute of Technology, Israel. Correspondence to: Moshe Eliasof <me532@cam.ac.uk>.

plethora of different layer designs has been proposed, each tailored to address specific challenges in the context of GNNs, such as limited expressive power (Xu et al., 2019; Morris et al., 2019; Maron et al., 2019) and oversmoothing (Nt & Maehara, 2019). Notably, analogously to architectures in other domains (He et al., 2016; Devlin et al., 2019), these GNN layers are often interleaved with normalization layers, as the integration of normalization methods has empirically proven beneficial in optimizing neural networks, facilitating convergence and enhancing generalization (Ioffe & Szegedy, 2015; Bjorck et al., 2018; Santurkar et al., 2018).

In practice, most existing GNN architectures employ standard normalization techniques, such as BatchNorm (Ioffe & Szegedy, 2015), LayerNorm (Ba et al., 2016), or InstanceNorm (Ulyanov et al., 2016). However, these widely adopted normalization techniques were not originally designed with graphs and GNNs in mind. Consequently, they may not effectively capture the unique characteristics of graph-structured data, and can also hinder the expressive power of the overall architecture (Cai et al., 2021). These observations highlight the need for graph-specific normalization layers.

Recent works have taken initial steps in this direction, mainly targeting the oversmoothing issue (Zhao & Akoglu, 2020; Yang et al., 2020; Zhou et al., 2020) or concerning the expressive power of the overall architecture (Cai et al., 2021; Chen et al., 2020). Despite the promise shown by these methods, a consensus on a single normalization technique optimal for diverse tasks remains elusive, with no single normalization method proving clearly superior across all benchmarks and scenarios.

**Our approach.** In this paper, we identify adaptivity to the input graph structure as a desirable property for an effective normalization layer for graph learning. Intuitively, this property ensures that the normalization is tailored to the specific input graph, capturing attributes such as the graph size, node degrees, and connectivity. Importantly, we claim and demonstrate that, given the limitations of practical GNNs, achieving full adaptivity requires expressive architectures that can detect and disambiguate graph substructures, thereby better adapting to input graphs.

Guided by this desirable property, which is absent in existing normalization methods, we introduce our proposed ap-

proach – GRANOLA (Graph Adaptive Normalization Layer). GRANOLA aims at dynamically adjusting node features at each layer by leveraging learnable characteristics of the neighborhood structure derived through the utilization of Random Node Features (RNF) (Murphy et al., 2019; Abboud et al., 2020; Puny et al., 2020; Sato et al., 2021; Dasoulas et al., 2021). More precisely, GRANOLA samples RNF and uses them in an additional GNN to obtain intermediate node representations. The intermediate representations are then used to scale and shift the node representations obtained by the preceding GNN layer.

We present theoretical results to support the main design choices of GRANOLA. Namely, we show that full adaptivity to the input graph of GRANOLA is a consequence of the additional expressive power of GNNs augmented with RNF (Abboud et al., 2020; Puny et al., 2020), which GRANOLA inherits, and is otherwise not captured by solely employing standard GNN layers or other normalizations.

Empirically, we show that GRANOLA significantly and consistently outperforms all existing standard as well as graph-specific normalization schemes on a variety of different graph benchmarks and architectures. Furthermore, GRANOLA proves to be the best performing method among all considered baselines that have the same time complexity of the most-widely adopted GNNs, namely the family of Message Passing Neural Networks (MPNNs).

**Contributions.** Our contributions are as follows: (1) We provide an overview of different normalization schemes in graph learning, outlining adaptivity as a desirable property of normalization layers that existing methods are missing, (2) We introduce GRANOLA, a novel normalization technique adjusting node features based on learnable characteristics of the neighborhood structure, (3) We present an intuitive theoretical analysis of our method, giving insight into the design choices we have made, and (4) We conduct an extensive empirical study, providing a thorough benchmarking of existing normalization methods, and showcasing the consistent superior performance of GRANOLA over existing normalization techniques across a variety of benchmarks.

## 2. Normalization layers for GNNs

In this section, we introduce our notations and the formulation of normalization layers in graphs.

### 2.1. Basic setup and definitions

Let  $G = (\mathbf{A}, \mathbf{X})$  denote graph with  $N \in \mathbb{N}$  nodes, where  $\mathbf{A} \in \mathbb{R}^{N \times N}$  is the adjacency matrix and  $\mathbf{X} \in \mathbb{R}^{N \times C}$  is the node feature matrix, with  $C \in \mathbb{N}$  being the feature dimensionality. Consider a batch of  $B \in \mathbb{N}$  graphs encoded by the adjacency matrices  $\{\mathbf{A}_b\}_{b=0}^{B-1}$ , and, for simplicity,

assume that all graphs in the batch have the same number of nodes  $N$ .

We consider a model composed of  $L$  GNN layers, with  $L \in \mathbb{N}$ . Each GNN layer is followed by a normalization layer NORM and an activation function  $\phi$ . At any layer  $\ell \in [L]$ , the output of the GNN layer for a batch of graphs consists of (intermediate) node representations, which can be gathered in a matrix  $\tilde{\mathbf{H}}^{(\ell)} \in \mathbb{R}^{B \times N \times C}$  (since all graphs have the same number of nodes per our assumption). These undergo a normalization and an activation layer, resulting in node representations denoted by  $\mathbf{H}^{(\ell)} \in \mathbb{R}^{B \times N \times C}$ , which serve as input of the next GNN layer, with  $\mathbf{H}^{(0)} := \mathbf{X}$ .<sup>1</sup> Throughout this paper, for any three-dimensional tensor, we use subscripts to denote access to a corresponding dimension. For example, the intermediate node representations of a single graph  $b \in [B]$  are denoted by  $\tilde{\mathbf{H}}_b^{(\ell)} \in \mathbb{R}^{N \times C}$ . Similarly, we denote by  $\tilde{h}_{b,n,c}^{(\ell)}$  the value of the feature  $c$  in node  $n$  of graph  $b$ , with  $c \in [C], n \in [N], b \in [B]$ .

Formally, the intermediate, *pre-normalized* node features for the  $b$ -th graph in the batch are defined as follows:

$$\tilde{\mathbf{H}}_b^{(\ell)} = \text{GNN}_{\text{LAYER}}^{(\ell-1)} \left( \mathbf{A}_b, \mathbf{H}_b^{(\ell-1)} \right). \quad (1)$$

Then, the overall update rule for the batch of  $B$  graphs can be written as

$$\mathbf{H}^{(\ell)} = \phi \left( \text{NORM} \left( \tilde{\mathbf{H}}^{(\ell)}; \ell \right) \right), \quad (2)$$

for  $\ell \in [L]$ . Equation (2) serves as a general blueprint, and in what follows we will show different ways to customize it in order to implement different existing normalization techniques.

We consider normalization layers based on the standardization (Larsen & Marx, 2005) of their inputs, as this represents the most common choice in widely-used normalizations. Generally, a standardization-based normalization layer first shifts each element  $\tilde{h}_{b,n,c}^{(\ell)}$  by some mean  $\mu_{b,n,c}$ , and then scales it by the corresponding standard deviation  $\sigma_{b,n,c}$ , i.e.,

$$\text{NORM}(\tilde{h}_{b,n,c}^{(\ell)}; \tilde{\mathbf{H}}^{(\ell)}, \ell) = \gamma_c^{(\ell)} \frac{\tilde{h}_{b,n,c}^{(\ell)} - \mu_{b,n,c}}{\sigma_{b,n,c}} + \beta_c^{(\ell)}, \quad (3)$$

where  $\gamma_c^{(\ell)}, \beta_c^{(\ell)} \in \mathbb{R}$  are learnable *affine* parameters, that do not depend on  $b$  nor  $n$ .

### 2.2. Current normalization layers for GNNs

The difference among different normalization schemes lies in the set of values used to compute the mean and standard deviation statistics for each element, or, more precisely,

<sup>1</sup>For simplicity and without loss of generality, we assume that the feature dimension of every GNN layer is always  $C$ .

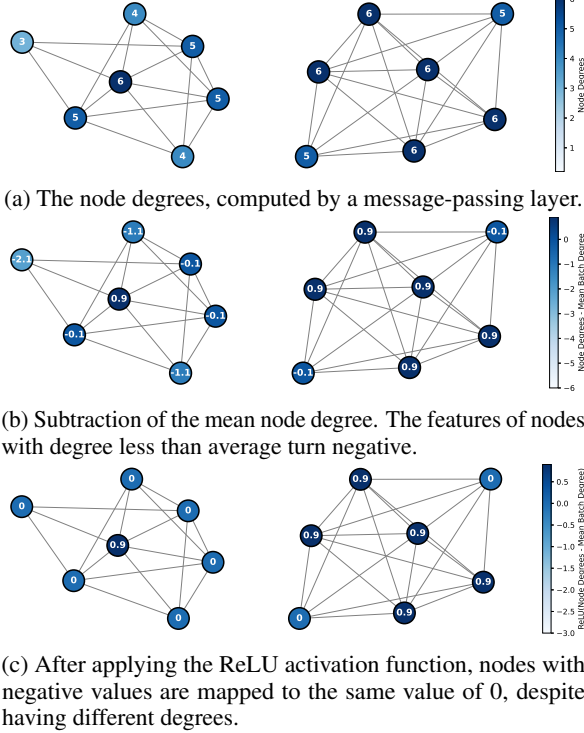


Figure 1: An example with a batch of two Erdős–Rényi random graphs, where subtracting the mean of the node features computed across the batch, as in BatchNorm and methods building upon it, results in the loss of capacity to compute node degrees.

across which dimensions of  $\tilde{\mathbf{H}}^{(\ell)}$  these computations are performed. We present them in the following, and visualize these differences in Figure 2.

**BatchNorm.** BatchNorm (Ioffe & Szegedy, 2015) computes the statistics across all nodes and all graphs in the batch, for each feature separately. Therefore, we have

$$\mu_{b,n,c} = \frac{1}{BN} \sum_{b=1}^B \sum_{n=1}^N \tilde{h}_{b,n,c}^{(\ell)}, \quad (4a)$$

$$\sigma_{b,n,c}^2 = \frac{1}{BN} \sum_{b=1}^B \sum_{n=1}^N (\tilde{h}_{b,n,c}^{(\ell)} - \mu_{b,n,c})^2, \quad (4b)$$

which implies that  $\mu_{b,n,c} = \mu_{b',n',c}$  for any  $b' \in [B]$  and any  $n' \in [N]$  (and similarly for  $\sigma_{b,n,c}^2$ ). Despite the widespread use of BatchNorm in graph learning (Xu et al., 2019), it is important to recognize scenarios where alternative normalization schemes might be more suitable. A concrete example illustrating this need is presented in Figure 1, focusing on the task of predicting the degree of each node.<sup>2</sup> In this example, BatchNorm, by subtracting the mean com-

<sup>2</sup>The node degree is a fundamental feature in graph-based methods. See for example Newman (2010).

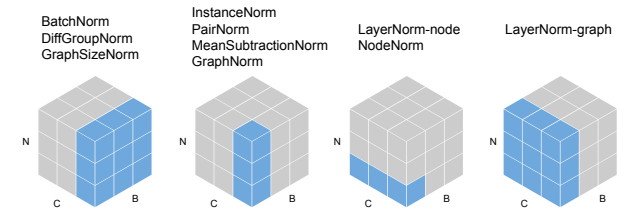


Figure 2: Illustration of Standard and Graph Normalization Layers. We denote by  $B$  the number of graphs (batch size), by  $N$  the number of nodes, and by  $C$  the number of channels (node features). For simplicity of presentation, we use the same number of nodes for all graphs in this figure. We color in blue the elements used to compute the statistics employed inside the normalization layer.

puted across the batch, results in negative values for nodes with outputs below the mean. The subsequent ReLU application, as standard practice (Xu et al., 2019; Kipf & Welling, 2017; Morris et al., 2019), zeros out these negative values, leading to predictions of 0 for such nodes, irrespective of their actual degree. Additional insights are further discussed in Example C.1 in Appendix C, where it is demonstrated that relying on the affine parameter  $\beta_c^{(\ell)}$  to shift the negative output does not provide a definitive solution, since  $\beta_c^{(\ell)}$  is the same for all graphs.

**InstanceNorm.** InstanceNorm (Ulyanov et al., 2016) behaves similarly to BatchNorm, but considers each graph separately, that is

$$\mu_{b,n,c} = \frac{1}{N} \sum_{n=1}^N \tilde{h}_{b,n,c}^{(\ell)}, \quad (5a)$$

$$\sigma_{b,n,c}^2 = \frac{1}{N} \sum_{n=1}^N (\tilde{h}_{b,n,c}^{(\ell)} - \mu_{b,n,c})^2, \quad (5b)$$

which implies that  $\mu_{b,n,c} = \mu_{b,n',c}$  for any  $n' \in [N]$  (and similarly for  $\sigma_{b,n,c}^2$ ). Notably, the example in Figure 1 can be extended to InstanceNorm by considering all graphs in the batch as disconnected components in a single graph, as we show in Example C.4 in Appendix C.

**LayerNorm.** LayerNorm (Ba et al., 2016) can be defined in two ways in the context of graphs (Fey & Lenssen, 2019b). The first, which we call *LayerNorm-node*, behaves similarly to LayerNorm in Transformer architectures (Vaswani et al., 2017), and computes statistics across the features for each node separately, that is

$$\mu_{b,n,c} = \frac{1}{C} \sum_{c=1}^C \tilde{h}_{b,n,c}^{(\ell)}, \quad (6a)$$

$$\sigma_{b,n,c}^2 = \frac{1}{C} \sum_{c=1}^C (\tilde{h}_{b,n,c}^{(\ell)} - \mu_{b,n,c})^2, \quad (6b)$$

and therefore  $\mu_{b,n,c} = \mu_{b,n,c'}$  for any  $c' \in [C]$  (and similarly for  $\sigma_{b,n,c}^2$ ). The second variant, which we call *LayerNorm-graph*, is similar to LayerNorm in Computer Vision (Wu & He, 2018), and computes statistics across the features and across all the nodes in each graph, that is

$$\mu_{b,n,c} = \frac{1}{NC} \sum_{n=1}^N \sum_{c=1}^C \tilde{h}_{b,n,c}^{(\ell)}, \quad (7a)$$

$$\sigma_{b,n,c}^2 = \frac{1}{NC} \sum_{n=1}^N \sum_{c=1}^C (\tilde{h}_{b,n,c}^{(\ell)} - \mu_{b,n,c})^2, \quad (7b)$$

and therefore  $\mu_{b,n,c} = \mu_{b,n',c'}$  for any  $n' \in [N]$  and any  $c' \in [C]$  (and similarly for  $\sigma_{b,n,c}^2$ ). Example C.5 in Appendix C presents a motivating example similar to Figure 1 in the context of LayerNorm.

**Graph-Specific Normalizations.** Various normalization methods tailored to graphs have been recently proposed. We categorize them based on which dimensions (the batch dimension  $B$ , the node dimension  $N$  within each graph, and the channel dimension  $C$ ) are used to compute the statistics employed inside the normalization layer. We illustrate this categorization in Figure 2. DiffGroupNorm (Zhou et al., 2020) and GraphSizeNorm (Dwivedi et al., 2023) normalize features considering nodes across different graphs, akin to BatchNorm. Similarly to InstanceNorm, PairNorm (Zhao & Akoglu, 2020) and MeanSubtractionNorm (Yang et al., 2020) shift the input by the mean computed per channel across all the nodes in the graph, with differences in the scaling strategies. GraphNorm (Cai et al., 2021) extends InstanceNorm by incorporating a multiplicative factor to the mean. NodeNorm (Zhou et al., 2021) behaves similarly to LayerNorm-node but only scales the input, without shifting it. We provide additional discussions and details in Appendix A and Appendix B, including methods that normalize the adjacency matrix before the GNN layers, which, however, fall outside the scope of the present work.

### 2.3. Discussion

In the previous subsection, we observed that current normalization schemes used within GNNs are mostly borrowed or adapted from other domains and that they possess several limitations: (i) Using BatchNorm and InstanceNorm (as well as many methods derived from them, including graph-specific methods) can limit the expressive power of GNNs that use them, preventing them from being able to represent even very simple functions such as computing nodes' degree; (ii) As shown in previous works, as well as in our experiments in Section 5, these methods do not provide a consistent behavior in downstream performance on different tasks and datasets.

One possible reason for these limitations is that the discussed methods use the same affine parameters in the nor-

---

#### Algorithm 1 GRANOLA Layer

---

**Input:** Node features  $\tilde{\mathbf{H}}_b^{(\ell)} \in \mathbb{R}^{N \times C}$ .

**Output:** Normalized features per node  $n \in [N]$  and channel  $c \in [C]$ .

- 1: Sample random node features  $\mathbf{R}_b^{(\ell)} \in \mathbb{R}^{N \times K}$ .
- 2: Compute  $\mathbf{Z}_b^{(\ell)} = \text{GNN}_{\text{NORM}}^{(\ell)}(\mathbf{A}_b, \tilde{\mathbf{H}}_b^{(\ell)} \oplus \mathbf{R}_b^{(\ell)})$ .
- 3: Compute affine parameters:  
 $\gamma_{b,n}^{(\ell)} = f_1^{(\ell)}(z_{b,n}^{(\ell)}), \quad \beta_{b,n}^{(\ell)} = f_2^{(\ell)}(z_{b,n}^{(\ell)})$ .
- 4: Compute mean and standard-deviation  $\mu_{b,n,c}$  and  $\sigma_{b,n,c}$  of  $\tilde{\mathbf{H}}_b^{(\ell)}$ .
- 5: Return  $\gamma_{b,n,c}^{(\ell)} \frac{\tilde{h}_{b,n,c}^{(\ell)} - \mu_{b,n,c}}{\sigma_{b,n,c}} + \beta_{b,n,c}^{(\ell)}$ .

---

malization process, irrespective of the input graph. Therefore, it might make sense to employ different (adaptive) normalization schemes based on the features and the connectivity of the input graph. We explore this concept in the next section and show that carefully accounting for the graph structure in the normalization process may enhance the expressive power of the GNN, overcoming the previously mentioned failure cases, and providing consistent experimental behavior and overall improved performance.

## 3. Method

The following section describes the proposed GRANOLA framework. We start with identifying adaptivity as a desired property in a graph normalization layer.

### 3.1. Adaptive normalization in GNNs

Adaptive normalization means that instead of using the same affine parameters (i.e.,  $\gamma_c^{(\ell)}$  and  $\beta_c^{(\ell)}$  in Equation (3) for all the nodes in all the graphs, the normalization method is able to determine specific parameters conditioned on the input graph. Importantly, in other domains, such as Computer Vision (Dumoulin et al., 2016; Huang & Belongie, 2017; Park et al., 2019; Zhu et al., 2020) and Signal Processing (Ogasawara et al., 2010; Passalis et al., 2019), adaptivity in normalization techniques has proven to be a valuable property.

In our GRANOLA, we accomplish this property by generating affine parameters by utilizing an additional *normalization* GNN that takes the original graph as input, similar to Hypernetworks (Ha et al., 2016) that generate weights for another network.

Importantly, to fully obtain graph adaptivity, the normalization GNN should have high expressive power, such that it can distinguish intricate substructures in different graphs. Due to the limited expressive power of message-passing neural networks (Morris et al., 2019; Xu et al., 2019), when

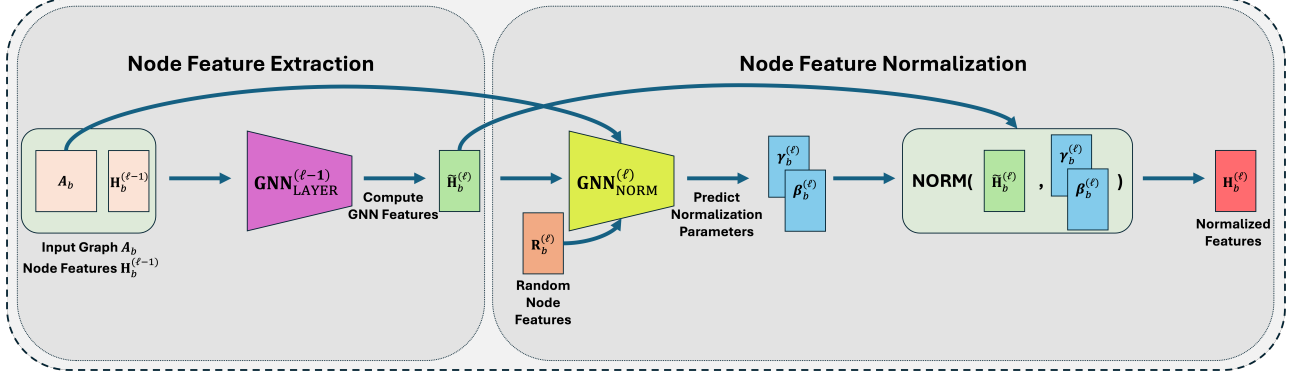


Figure 3: Illustration of a GRANOLA layer. Given node features  $H_b^{(\ell-1)}$  and the adjacency matrix  $A_b$ , we feed them to a  $\text{GNN}_{\text{LAYER}}^{(\ell-1)}$  to extract updated node features. Then, we predict normalization parameters using  $\text{GNN}_{\text{NORM}}^{(\ell)}$ , which takes sampled RNF  $\mathbf{R}_b^{(\ell)}$ , the updated features  $\tilde{H}_b^{(\ell)}$ , and the adjacency matrix  $A_b$ . Considering  $A_b$  and  $\tilde{H}_b^{(\ell)}$  results in graph-adaptivity, and including  $\mathbf{R}_b^{(\ell)}$  enhances the expressiveness of GRANOLA, fulfilling the desiderata discussed in Section 3.1.

designing GRANOLA, we advocate for using GNNs with increased expressiveness. Notably, most expressive GNNs come at the expense of significantly increased computational complexity, such as Subgraph GNNs (Bevilacqua et al., 2022), which might make our GRANOLA too computationally demanding. For this reason, we parameterize the normalization GNN using an MPNN augmented with Random Node Features (RNF), which provide strong function approximation guarantees (Abboud et al., 2020; Puny et al., 2020) while retaining the efficiency of standard MPNNs.

### 3.2. GRANOLA

We are now ready to describe our GRANOLA approach, which includes the utilization of an additional GNN to compute the affine parameters and the integration of RNF (Sato et al., 2021). These affine parameters are then employed to normalize node representations obtained by the GNN layer preceding the normalization. An overview of GRANOLA is visualized in Figure 3 and described in Algorithm 1. First, we describe the basic approach, and then we discuss two specific variants.

**Basic GRANOLA Layer.** At any given layer  $\ell \in [L]$ , for each graph  $b \in [B]$ , we sample RNF  $\mathbf{R}_b^{(\ell)} \in \mathbb{R}^{N \times K}$ ,  $K \in \mathbb{N}$ , from some joint continuous and bounded probability distribution,  $\mathbf{R}_b^{(\ell)} \sim \mathcal{D}$ . Then, we concatenate  $\mathbf{R}_b^{(\ell)}$  with the intermediate node features predicted by our GNN layer  $\tilde{H}_b^{(\ell)}$  (Equation (1)), and pass the resulting feature matrix through an additional GNN, i.e.,

$$\mathbf{Z}_b^{(\ell)} = \text{GNN}_{\text{NORM}}^{(\ell)}(\mathbf{A}_b, \tilde{H}_b^{(\ell)} \oplus \mathbf{R}_b^{(\ell)}), \quad (8)$$

where  $\oplus$  denotes feature-wise concatenation, and  $\text{GNN}_{\text{NORM}}^{(\ell)}$  is a shallow GNN architecture, with  $L_{\text{NORM}}^{(\ell)}$  layers. The

affine parameters are then computed from  $\mathbf{Z}_b^{(\ell)} \in \mathbb{R}^{N \times C}$ , that is

$$\gamma_{b,n}^{(\ell)} = f_1^{(\ell)}(z_{b,n}^{(\ell)}), \quad \beta_{b,n}^{(\ell)} = f_2^{(\ell)}(z_{b,n}^{(\ell)}). \quad (9)$$

where  $f_1^{(\ell)}, f_2^{(\ell)}$  are learnable functions (e.g., MLPs), and  $\gamma_{b,n}^{(\ell)}, \beta_{b,n}^{(\ell)} \in \mathbb{R}^C$ . Then, a GRANOLA layer is defined as

$$\text{NORM}(\tilde{h}_{b,n,c}^{(\ell)}; \tilde{\mathbf{H}}^{(\ell)}, \ell) = \gamma_{b,n,c}^{(\ell)} \frac{\tilde{h}_{b,n,c}^{(\ell)} - \mu_{b,n,c}}{\sigma_{b,n,c}} + \beta_{b,n,c}^{(\ell)}, \quad (10)$$

where  $\mu_{b,n,c}$  and  $\sigma_{b,n,c}$  are the mean and std of  $\tilde{\mathbf{H}}^{(\ell)}$ , computed per node across the feature dimension, exactly as in LayerNorm-node (Equations (6a) and (6b)). We highlight here a noticeable difference compared to standard normalization formulations, as presented in Equation (3): in GRANOLA,  $\gamma_{b,n,c}^{(\ell)}, \beta_{b,n,c}^{(\ell)}$  not only depend on  $c$ , but they also have a dependency on  $b$  and  $n$  and indeed vary for different graphs and nodes. Notably, this is possible because our normalization is adaptive to the input graph. Methods that disregard this information are compelled to use the same learnable embeddings for all graphs, as they operate without knowledge of the specific input graph being considered.

**GRANOLA-MS.** Equation (10) can be specialized to the case where the affine parameters correspond to the mean and standard deviation computed per node across the feature dimension of  $\mathbf{Z}_b^{(\ell)}$ . That is,

$$\gamma_{b,n,c}^{(\ell)} = \frac{1}{C} \sum_{c=1}^C z_{b,n,c}^{(\ell)}, \quad (11a)$$

$$\beta_{b,n,c}^{(\ell)} = \frac{1}{C} \sum_{c=1}^C (z_{b,n,c}^{(\ell)} - \gamma_{b,n,c}^{(\ell)})^2. \quad (11b)$$

We refer to this variant of Equation (10) which uses the pre-defined mean and standard deviation functions in Equations (11a) and (11b) for  $f_1^{(\ell)}, f_2^{(\ell)}$  as GRANOLA-MS, where MS stands indeed for mean and standard deviation. The idea behind GRANOLA-MS is to explicitly align the node-wise mean and variance of  $\tilde{\mathbf{H}}_b^{(\ell)}$  to match those of  $\mathbf{Z}_b^{(\ell)}$ . Note that, while GRANOLA-MS follows a predefined realization of  $f_1$  and  $f_2$  by using the mean and standard-deviation, it is still a learnable normalization technique, as  $\mathbf{Z}_b^{(\ell)}$  is learned in Equation (8). In Appendix G.4, we provide empirical comparisons with this specialized case.

**GRANOLA-NO-RNF.** Furthermore, we consider an additional variant of GRANOLA that does not sample RNF and instead uses only  $\tilde{\mathbf{H}}_b^{(\ell)}$  to obtain  $\mathbf{Z}_b^{(\ell)}$  in Equation (8), which therefore becomes

$$\mathbf{Z}_b^{(\ell)} = \text{GNN}_{\text{NORM}}^{(\ell)}(\mathbf{A}, \tilde{\mathbf{H}}_b^{(\ell)}). \quad (12)$$

We refer to this variant as GRANOLA-NO-RNF, as it allows us to directly quantify the contribution of the graph-adaptivity property offered by utilizing  $\text{GNN}_{\text{NORM}}^{(\ell)}$ , and the expressiveness offered by augmenting it with RNF as in Equation (8).

We conclude by remarking that both GRANOLA and its variants, GRANOLA-MS and GRANOLA-NO-RNF, do not impact the asymptotic time complexity of standard MPNNs, which remains linear in the number of nodes and edges, as we show in Appendix F.

## 4. Theoretical Analysis

In this section, we explain the main design choices taken in the development of GRANOLA. Specifically, we elaborate on the advantages obtained by utilizing RNF as part of the normalization scheme as opposed to relying solely on the node features. We assume that all GNN layers, including those within GRANOLA (Equation (8)) are message-passing layers, as the ones in Xu et al. (2019); Morris et al. (2019).

**GRANOLA can default to standard RNF-augmented MPNNs.** We start by observing that the integration of our GRANOLA in an MPNN allows to easily default to an MPNN augmented with RNF (Sato et al., 2021), as we formalize in Proposition D.1 in Appendix D. The idea of the proof lies in the ability of the first normalization layer to default to outputting its input RNF, enabling the rest of the architecture to function as an MPNN augmented with these RNF. The significance of this result lies in the fact that MPNN + GRANOLA inherits the  $(\epsilon, \delta)$ -universal approximation properties previously proved for MPNNs augmented with RNF (Abboud et al., 2020; Puny et al., 2020). As an example, the above result allows an MPNN + GRANOLA to approximate structural properties of the graph, such as

counting the number of triangles, or substructures in general, each node is involved in. Notably, it has been proven that standard MPNNs can *not* count many of these substructures (Chen et al., 2020).

**The importance of RNF.** While GRANOLA employs RNF to compute the normalization affine parameters  $\gamma_{b,n,c}^{(\ell)}$  and  $\beta_{b,n,c}^{(\ell)}$ , the same procedure can be applied without the use of RNF, a variant we denoted as GRANOLA-NO-RNF in Section 3 (Equation (12)). However, we theoretically demonstrate next that an MPNN + GRANOLA-NO-RNF not only loses the universal approximation properties, but is also not more expressive than standard MPNNs.

**Proposition 4.1** (RNF are necessary in GRANOLA for increased expressive power). *Let  $N$  be a natural number and consider all graphs of size  $N$ . An MPNN with GRANOLA-NO-RNF (Equation (12)) is not more expressive than a standard MPNN.*

Proposition 4.1 is proven by showing that an MPNN with GRANOLA-NO-RNF can be implemented by a standard MPNN, and, therefore, its expressive power is bounded by the expressive power of a standard MPNN. The proof can be found in Appendix D. This limitation underscores the significance of RNF within GRANOLA. Furthermore, our experiments in Section 5 show that omitting the RNF within the normalization results in degraded performance compared to that of our complete GRANOLA, as GRANOLA always outperforms GRANOLA-NO-RNF. Finally, we emphasize that this theoretical result underscores the necessity of RNF for increased expressiveness and, consequently, for ensuring complete adaptivity to the input graph, as discussed in Section 3.1.

**Relation to expressive GNNs.** The results in this section highlight the connection between GRANOLA and expressive GNNs, as our method inherits enhanced expressiveness of MPNNs augmented with RNF. Notably, while MPNNs with RNF have demonstrated theoretical improvements in expressiveness, their practical performance on real-world datasets has not consistently reflected these benefits (Eliasof et al., 2023). Our experimental results indicate that GRANOLA serves as a valuable bridge between theory and practice, addressing the gap between theoretical expressiveness and practical utility by effectively incorporating RNF within the normalization process. Finally, we conclude this section by remarking that  $\text{GNN}_{\text{NORM}}^{(\ell)}$  in Equation (8) can be modified to be any other expressive architecture, and our design choice was mainly guided by the computational practicality of RNF, that allows GRANOLA to offer improved expressiveness in theory and practical performance improvement, while retaining the linear complexity of MPNNs, as discussed in Appendix F. We refer the reader to Morris et al. (2021) for a survey on expressive methods.

Table 1: Comparison of GRANOLA with various baselines on the ZINC-12K graph dataset. All methods obey to the 500k parameter budget. The top three methods are marked by **First**, **Second**, **Third**.

Method	ZINC (MAE $\downarrow$ )
<b>EXPRESSIVE GNNs</b>	
GSN (Bouritsas et al., 2022)	<b>0.101</b> $\pm$ 0.010
CIN (Bodnar et al., 2021a)	<b>0.079</b> $\pm$ 0.006
<b>NATURAL BASELINES</b>	
GIN + BatchNorm + RNF-PE (Sato et al., 2021)	0.1621 $\pm$ 0.014
GIN + RNF-NORM	0.1562 $\pm$ 0.013
<b>STANDARD NORMALIZATION LAYERS</b>	
GIN + BatchNorm (Xu et al., 2019)	0.1630 $\pm$ 0.004
GIN + InstanceNorm (Ulyanov et al., 2016)	0.2984 $\pm$ 0.017
GIN + LayerNorm-node (Ba et al., 2016)	0.1649 $\pm$ 0.009
GIN + LayerNorm-graph (Ba et al., 2016)	0.1609 $\pm$ 0.014
GIN + Identity	0.2209 $\pm$ 0.018
<b>GRAPH NORMALIZATION LAYERS</b>	
GIN + PairNorm (Zhao & Akoglu, 2020)	0.3519 $\pm$ 0.008
GIN + MeanSubtractionNorm (Yang et al., 2020)	0.1632 $\pm$ 0.021
GIN + DiffGroupNorm (Zhou et al., 2020)	0.2705 $\pm$ 0.024
GIN + NodeNorm (Zhou et al., 2021)	0.2119 $\pm$ 0.017
GIN + GraphNorm (Cai et al., 2021)	0.3104 $\pm$ 0.012
GIN + GraphSizeNorm (Dwivedi et al., 2023)	0.1931 $\pm$ 0.016
GIN + SuperNorm (Chen et al., 2023)	0.1574 $\pm$ 0.018
GIN + GRANOLA-NO-RNF	0.1497 $\pm$ 0.008
<b>GIN + GRANOLA</b>	<b>0.1203</b> $\pm$ 0.006

## 5. Experimental Results

In this section, we empirically evaluate the performance of GRANOLA. In particular, we seek to address the following questions: (1) Can GRANOLA outperform other graph normalization methods? (2) Does GRANOLA achieve better performance than its natural baselines that also leverage RNF? (3) How does our method perform compared with expressive GNNs? (4) How does GRANOLA compare to its variant GRANOLA-NO-RNF, which does not leverage RNF in the normalization process?

In what follows, we present our main results and refer to Appendix E for further experiments and details.

**Baselines.** For each task, we consider the following baselines: (1) Expressive GNNs; (2) MPNNs with standard normalization layers such as BatchNorm, InstanceNorm, LayerNorm-node, LayerNorm-graph and Identity (i.e., no normalization in between layers), as well as (3) graph-designated normalization layers like PairNorm, MeanSubtractionNorm, DiffGroupNorm, NodeNorm, GraphNorm and GraphSizeNorm, SuperNorm. Furthermore, we consider (4) natural baselines, namely: (i) RNF as a positional encoding (RNF-PE), where we augment only the initial input features with RNF, as in Sato et al. (2021); (ii) The normalization that uses only RNF, without any message passing layer inside the normalization, to compute the normalization affine parameters  $\gamma_{b,n,c}^{(\ell)}$  and  $\beta_{b,n,c}^{(\ell)}$ . This is achieved

by considering  $\mathbf{Z}_b^{(\ell)} = \mathbf{R}_b^{(\ell)}$  in Equation (8). We denote this baseline by RNF-NORM. For a fair comparison, in all the baselines, as well as in our method, we employ the maximally-expressive (within the MPNNs family) GIN or GINE layers (Xu et al., 2019), depending on the presence of edge features.

In Appendix G.4, we provide additional comparisons with other methods, ranging from classical methods to Subgraph GNNs, on all the datasets considered in this section, as well as a comparison with the variant GRANOLA-MS discussed in Equation (11). We also provide ablation studies in Appendix G.1 and Appendix G.2 that show the importance of the normalization design of our GRANOLA. Lastly, we show in Appendix G.3 that GRANOLA can also be coupled with expressive architectures like GSN (Bouritsas et al., 2022), improving their results.

**ZINC.** We experiment with the ZINC-12K molecular dataset (Sterling & Irwin, 2015; Gómez-Bombarelli et al., 2018; Dwivedi et al., 2023), where the goal is to regress the solubility of molecules. As can be seen from Table 1, GRANOLA achieves significantly lower (better) mean-absolute-error compared to existing standard and graph-designated normalization layers, while outperforming all its natural baselines. Moreover, GRANOLA reduces the performance gap between MPNNs, which have linear complexity, and expressive GNNs, which are more computationally expensive, demonstrating to be the best performing model with the same time complexity of a standard MPNN.

**OGB.** We test our GRANOLA on the OGB graph benchmark collection (Hu et al., 2020). In Table 2, we show the performance of GRANOLA compared with the various baselines. Notably, GRANOLA consistently improves over existing standard normalization methods while retaining similar asymptotic complexity. For instance, on MOLBACE, we achieve an accuracy of 79.92% compared to 72.97% when using BatchNorm, an improvement of 6.95%. Compared with graph-designated normalization methods, GRANOLA also offers a consistent improvement. As an example, on MOLESOL we obtain a root-squared-mean-error of (lower is better) of 0.960, compared to the second best graph normalization layer, GraphNorm, that achieves 1.044. It is also noteworthy to mention the performance gap between GRANOLA and its natural baselines, such as RNF-PE, which emphasizes the practical benefit of the design of GRANOLA.

**TUDatasets.** We experimented with popular datasets from the TUD (Morris et al., 2020) repository. Our results are reported in Table 3, suggesting two main takeaways. (1) GRANOLA consistently achieves higher accuracy compared to its natural baselines, as well as standard and graph-designated normalization techniques. For example, on the NCI109 dataset, GRANOLA achieves an accuracy of 83.7%, compared to the second-best normalization technique, Graph-

Table 2: A comparison of GRANOLA to natural baselines, standard and graph normalization layers, demonstrating the practical advantages of our approach. The top three methods are marked by **First**, **Second**, **Third**.

Method ↓ / Dataset →	MOLESOL RMSE ↓	MOLTOX21 ROC-AUC ↑	MOLBACE ROC-AUC ↑	MOLHIV ROC-AUC ↑
<b>EXPRESSIVE GNNs</b>				
GSN (Bouritsas et al., 2022)	–	–	–	<b>80.39</b> ±0.90
CIN (Bodnar et al., 2021a)	–	–	–	<b>80.94</b> ±0.57
<b>NATURAL BASELINES</b>				
GIN + BatchNorm + RNF-PE (Sato et al., 2021)	1.052±0.041	<b>75.14</b> ±0.67	74.28±3.80	75.98±1.63
GIN + RNF-NORM	<b>1.039</b> ±0.040	<b>75.12</b> ±0.92	<b>77.96</b> ±4.36	77.61±1.64
<b>STANDARD NORMALIZATION LAYERS</b>				
GIN + BatchNorm (Xu et al., 2019)	1.173±0.057	74.91±0.51	72.97±4.00	75.58±1.40
GIN + InstanceNorm (Ulyanov et al., 2016)	1.099±0.038	73.82±0.96	74.86±3.37	76.88±1.93
GIN + LayerNorm-node (Ba et al., 2016)	1.058±0.024	74.81±0.44	<b>77.12</b> ±2.70	75.24±1.71
GIN + LayerNorm-graph (Ba et al., 2016)	1.061±0.043	75.03±1.24	76.49±4.07	76.13±1.84
GIN + Identity	1.164±0.059	73.34±1.08	72.55±2.98	71.89±1.32
<b>GRAPH NORMALIZATION LAYERS</b>				
GIN + PairNorm (Zhao & Akoglu, 2020)	1.084±0.031	73.27±1.05	75.11±4.24	76.18±1.47
GIN + MeanSubtractionNorm (Yang et al., 2020)	1.062±0.045	74.98±0.62	76.36±4.47	76.37±1.40
GIN + DiffGroupNorm (Zhou et al., 2020)	1.087±0.063	74.48±0.76	75.96±3.79	74.37±1.68
GIN + NodeNorm (Zhou et al., 2021)	1.068±0.029	73.27±0.83	75.67±4.03	75.50±1.32
GIN + GraphNorm (Cai et al., 2021)	1.044±0.027	73.54±0.80	73.23±3.88	78.08±1.16
GIN + GraphSizeNorm (Dwivedi et al., 2023)	1.121±0.051	74.07±0.30	76.18±3.52	75.44±1.51
GIN + SuperNorm (Chen et al., 2023)	<b>1.037</b> ±0.044	75.08±0.98	75.12±3.38	76.55±1.76
GIN + GRANOLA-NO-RNF	1.088±0.032	75.87±0.72	76.23±2.06	77.09±1.49
GIN + GRANOLA	<b>0.960</b> ±0.020	<b>77.19</b> ±0.85	<b>79.92</b> ±2.56	<b>78.98</b> ±1.17

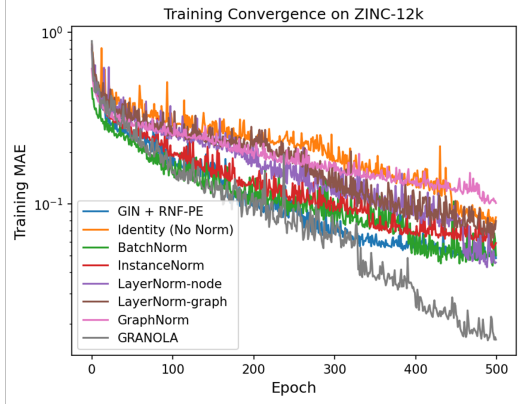


Figure 4: Training convergence of GRANOLA compared with existing normalization techniques show that GRANOLA achieves faster convergence and overall lower (better) MAE.

Norm, with an accuracy 82.4%. (2) Compared with expressive GNNs, GRANOLA yields competitive results, and in 3 out of 5 datasets, GRANOLA achieves better performance.

**Training Convergence of GRANOLA.** In addition to improved downstream task performance being one of the main benefits of a normalization layer, accelerated training convergence is also an important desired property (Ioffe &

Szegedy, 2015; Cai et al., 2021). Figure 4 shows that GRANOLA offers better convergence and lower MAE compared to other methods.

**Discussion.** Our experimental results cover standard normalization layers, as well as recent graph normalization methods, evaluated on 11 datasets from diverse sources, and applied to various tasks. Throughout all experiments, a common theme is the performance *consistency* of GRANOLA. Specifically, GRANOLA always improves over its natural baselines and other normalization techniques across all datasets. In contrast, other existing methods exhibit less clear trends in their performance. While some methods achieve competitive results on certain datasets, they may struggle on others. Notable examples are GraphNorm and PairNorm, which, despite offering improved performance compared to standard BatchNorm on most of the OGB datasets, show worse results on ZINC-12K. Furthermore, standard normalization layers also lack consistency. A case point is InstanceNorm, which is beneficial in some OGB datasets, yet, it does not offer favorable results on ZINC-12K.

## 6. Conclusions

In this paper, we discuss and benchmark the existing landscape of feature normalization techniques in Graph Neural Networks (GNNs). Despite recent advances in designing

Table 3: Graph classification accuracy (%)  $\uparrow$  on TUDatasets. – indicates the results was not reported in the original paper. The top three methods are marked by **First**, **Second**, **Third**.

Method $\downarrow$ / Dataset $\rightarrow$	MUTAG	PTC	PROTEINS	NCI1	NCI109
<b>EXPRESSIVE GNNs</b>					
GSN (Bouritsas et al., 2022)	<b>92.2</b> $\pm$ 7.5	<b>68.2</b> $\pm$ 7.2	76.6 $\pm$ 5.0	<b>83.5</b> $\pm$ 2.0	–
SIN (Bodnar et al., 2021b)	–	–	76.4 $\pm$ 3.3	82.7 $\pm$ 2.1	–
CIN (Bodnar et al., 2021a)	<b>92.7</b> $\pm$ 6.1	<b>68.2</b> $\pm$ 5.6	<b>77.0</b> $\pm$ 4.3	<b>83.6</b> $\pm$ 1.4	<b>84.0</b> $\pm$ 1.6
<b>NATURAL BASELINES</b>					
GIN + BatchNorm + RNF-PE (Sato et al., 2021)	90.8 $\pm$ 4.8	64.4 $\pm$ 6.7	74.1 $\pm$ 2.6	82.1 $\pm$ 1.5	81.3 $\pm$ 1.1
GIN + RNF-NORM	88.9 $\pm$ 5.1	67.1 $\pm$ 4.3	76.4 $\pm$ 4.8	81.8 $\pm$ 2.2	81.9 $\pm$ 2.5
<b>STANDARD NORMALIZATION LAYERS</b>					
GIN + BatchNorm (Xu et al., 2019)	89.4 $\pm$ 5.6	64.6 $\pm$ 7.0	76.2 $\pm$ 2.8	82.7 $\pm$ 1.7	82.2 $\pm$ 1.6
GIN + InstanceNorm (Ulyanov et al., 2016)	90.5 $\pm$ 7.8	64.7 $\pm$ 5.9	76.5 $\pm$ 3.9	81.2 $\pm$ 1.8	81.8 $\pm$ 1.6
GIN + LayerNorm-node (Ba et al., 2016)	90.1 $\pm$ 5.9	65.3 $\pm$ 4.7	76.2 $\pm$ 3.0	81.9 $\pm$ 1.5	82.0 $\pm$ 2.1
GIN + Layernorm-graph (Ba et al., 2016)	90.4 $\pm$ 6.1	66.4 $\pm$ 6.5	76.1 $\pm$ 4.9	82.0 $\pm$ 1.6	81.5 $\pm$ 1.3
GIN + Identity	87.9 $\pm$ 7.8	63.1 $\pm$ 7.2	75.8 $\pm$ 6.3	81.3 $\pm$ 2.1	80.6 $\pm$ 1.7
<b>GRAPH NORMALIZATION LAYERS</b>					
GIN + PairNorm (Zhao & Akoglu, 2020)	87.8 $\pm$ 7.1	67.1 $\pm$ 6.3	76.7 $\pm$ 4.8	75.8 $\pm$ 2.1	75.3 $\pm$ 1.4
GIN + MeanSubtractionNorm (Yang et al., 2020)	90.1 $\pm$ 5.4	<b>68.0</b> $\pm$ 5.9	76.4 $\pm$ 4.6	79.2 $\pm$ 1.2	79.0 $\pm$ 1.1
GIN + DiffGroupNorm (Zhou et al., 2020)	87.8 $\pm$ 7.6	67.4 $\pm$ 6.8	76.9 $\pm$ 4.3	77.2 $\pm$ 2.6	77.1 $\pm$ 1.9
GIN + NodeNorm (Zhou et al., 2021)	88.3 $\pm$ 7.0	65.1 $\pm$ 8.3	74.5 $\pm$ 4.6	81.2 $\pm$ 1.4	79.4 $\pm$ 1.0
GIN + GraphNorm (Cai et al., 2021)	<b>91.6</b> $\pm$ 6.5	64.9 $\pm$ 7.5	<b>77.4</b> $\pm$ 4.9	81.4 $\pm$ 2.4	82.4 $\pm$ 1.7
GIN + GraphSizeNorm (Dwivedi et al., 2023)	88.2 $\pm$ 6.3	<b>68.0</b> $\pm$ 8.1	<b>77.0</b> $\pm$ 5.0	79.8 $\pm$ 1.5	80.1 $\pm$ 1.8
GIN + SuperNorm (Chen et al., 2023)	89.3 $\pm$ 5.6	64.7 $\pm$ 3.9	76.1 $\pm$ 4.7	83.0 $\pm$ 1.5	<b>82.8</b> $\pm$ 1.7
GIN + GRANOLA-NO-RNF	89.7 $\pm$ 5.4	65.8 $\pm$ 5.7	76.6 $\pm$ 2.5	83.1 $\pm$ 1.2	83.0 $\pm$ 1.5
<b>GIN + GRANOLA</b>	<b>92.2</b> $\pm$ 4.6	<b>69.9</b> $\pm$ 4.5	<b>77.5</b> $\pm$ 3.7	<b>84.0</b> $\pm$ 1.7	<b>83.7</b> $\pm$ 1.6

graph-specific normalization techniques, the optimal choice remains unclear, with methods not offering consistent performance improvements across tasks. To address this challenge, we propose a desirable property of graph normalization layers, namely adaptivity to the input graph, and argue that it can be obtained only with expressive architectures. To incorporate this property, we present GRANOLA, a normalization layer that adjusts node features based on the specific characteristics of the graph, leveraging Random Node Features (RNF). Our theoretical analyses support the design choices of GRANOLA, demonstrating its increased expressiveness. Empirical evaluations across diverse graph benchmarks consistently highlight the superior performance of GRANOLA over existing normalization techniques, as well as other baselines with the same time complexity.

**Limitations.** Although GRANOLA exhibits promising results and outperforms all existing normalization techniques, there are areas for potential improvement and exploration in future research. For instance, investigating alternative designs for  $\text{GNN}_{\text{NORM}}^{(\ell)}$  could provide insights into further enhancing the model’s performance, as, in certain datasets such as ZINC, there is still a gap between GRANOLA and expressive GNNs. Additionally, assessing the generalization capabilities of GRANOLA across diverse datasets and graph structures remains an intriguing avenue for future investigation.

## References

Abboud, R., Ceylan, I. I., Grohe, M., and Lukasiewicz, T. The surprising power of graph neural networks with random node initialization. *arXiv preprint arXiv:2010.01179*, 2020.

Awais, M., Iqbal, M. T. B., and Bae, S.-H. Revisiting internal covariate shift for batch normalization. *IEEE Transactions on Neural Networks and Learning Systems*, 32(11):5082–5092, 2020.

Ba, J. L., Kiros, J. R., and Hinton, G. E. Layer normalization. *arXiv preprint arXiv:1607.06450*, 2016.

Bevilacqua, B., Frasca, F., Lim, D., Srinivasan, B., Cai, C., Balamurugan, G., Bronstein, M. M., and Maron, H. Equivariant subgraph aggregation networks. In *International Conference on Learning Representations*, 2022.

Bevilacqua, B., Eliasof, M., Meirom, E., Ribeiro, B., and Maron, H. Efficient subgraph gnns by learning effective selection policies. *arXiv preprint arXiv:2310.20082*, 2023.

Biewald, L. Experiment tracking with weights and biases, 2020. Software available from wandb.com.

Bjorck, N., Gomes, C. P., Selman, B., and Weinberger, K. Q. Understanding batch normalization. *Advances in neural information processing systems*, 31, 2018.

Bodnar, C., Frasca, F., Otter, N., Wang, Y. G., Liò, P., Montúfar, G., and Bronstein, M. Weisfeiler and lehman go cellular: CW networks. In *Advances in Neural Information Processing Systems*, volume 34, 2021a.

Bodnar, C., Frasca, F., Wang, Y. G., Otter, N., Montúfar, G., Lio, P., and Bronstein, M. Weisfeiler and lehman go topological: Message passing simplicial networks. *ICML*, 2021b.

Bouritsas, G., Frasca, F., Zafeiriou, S., and Bronstein, M. M. Improving graph neural network expressivity via subgraph isomorphism counting. *IEEE Transactions on Pattern Analysis and Machine Intelligence*, 2022.

Cai, T., Luo, S., Xu, K., He, D., Liu, T.-y., and Wang, L. Graphnorm: A principled approach to accelerating graph neural network training. In *International Conference on Machine Learning*, pp. 1204–1215. PMLR, 2021.

Chen, K., Liu, S., Zhu, T., Qiao, J., Su, Y., Tian, Y., Zheng, T., Zhang, H., Feng, Z., Ye, J., et al. Improving expressivity of gnns with subgraph-specific factor embedded normalization. In *Proceedings of the 29th ACM SIGKDD Conference on Knowledge Discovery and Data Mining*, pp. 237–249, 2023.

Chen, Y., Tang, X., Qi, X., Li, C.-G., and Xiao, R. Learning graph normalization for graph neural networks. *Neurocomputing*, 493:613–625, 2022.

Chen, Z., Chen, L., Villar, S., and Bruna, J. Can graph neural networks count substructures? *Advances in neural information processing systems*, 33:10383–10395, 2020.

Corso, G., Cavalleri, L., Beaini, D., Liò, P., and Veličković, P. Principal neighbourhood aggregation for graph nets. In *Advances in Neural Information Processing Systems*, 2020.

Cotta, L., Morris, C., and Ribeiro, B. Reconstruction for powerful graph representations. In *NeurIPS*, 2021.

Dasoulas, G., Santos, L. D., Scaman, K., and Virmaux, A. Coloring graph neural networks for node disambiguation. In *Proceedings of the Twenty-Ninth International Conference on International Joint Conferences on Artificial Intelligence*, pp. 2126–2132, 2021.

Devlin, J., Chang, M.-W., Lee, K., and Toutanova, K. Bert: Pre-training of deep bidirectional transformers for language understanding. In *North American Chapter of the Association for Computational Linguistics*, 2019.

Dumoulin, V., Shlens, J., and Kudlur, M. A learned representation for artistic style. *arXiv preprint arXiv:1610.07629*, 2016.

Dwivedi, V. P., Luu, A. T., Laurent, T., Bengio, Y., and Bresson, X. Graph neural networks with learnable structural and positional representations. In *International Conference on Learning Representations*, 2022.

Dwivedi, V. P., Joshi, C. K., Luu, A. T., Laurent, T., Bengio, Y., and Bresson, X. Benchmarking graph neural networks. *Journal of Machine Learning Research*, 24(43):1–48, 2023.

Eliasof, M., Frasca, F., Bevilacqua, B., Treister, E., Chechik, G., and Maron, H. Graph positional encoding via random feature propagation. In *International Conference on Machine Learning*, pp. 9202–9223, 2023.

Fey, M. and Lenssen, J. E. Fast graph representation learning with PyTorch Geometric. In *ICLR Workshop on Representation Learning on Graphs and Manifolds*, 2019a.

Fey, M. and Lenssen, J. E. Fast graph representation learning with PyTorch Geometric. In *ICLR Workshop on Representation Learning on Graphs and Manifolds*, 2019b.

Frasca, F., Bevilacqua, B., Bronstein, M., and Maron, H. Understanding and extending subgraph gnns by rethinking their symmetries. *Advances in Neural Information Processing Systems*, 35:31376–31390, 2022.

Ghiasi, G., Lee, H., Kudlur, M., Dumoulin, V., and Shlens, J. Exploring the structure of a real-time, arbitrary neural artistic stylization network. *arXiv preprint arXiv:1705.06830*, 2017.

Goodfellow, I., Pouget-Abadie, J., Mirza, M., Xu, B., Warde-Farley, D., Ozair, S., Courville, A., and Bengio, Y. Generative adversarial nets. *Advances in neural information processing systems*, 27, 2014.

Gómez-Bombarelli, R., Wei, J. N., Duvenaud, D., Hernández-Lobato, J. M., Sánchez-Lengeling, B., Sheberla, D., Aguilera-Iparraguirre, J., Hirzel, T. D., Adams, R. P., and Aspuru-Guzik, A. Automatic chemical design using a data-driven continuous representation of molecules. *ACS Central Science*, 4(2):268–276, Jan 2018.

Ha, D., Dai, A., and Le, Q. V. Hypernetworks, 2016.

He, K., Zhang, X., Ren, S., and Sun, J. Identity mappings in deep residual networks. In *Computer Vision–ECCV 2016: 14th European Conference, Amsterdam, The Netherlands, October 11–14, 2016, Proceedings, Part IV 14*, pp. 630–645. Springer, 2016.

Hu, W., Fey, M., Zitnik, M., Dong, Y., Ren, H., Liu, B., Catasta, M., and Leskovec, J. Open graph benchmark: Datasets for machine learning on graphs. In *Advances in Neural Information Processing Systems*, volume 33, 2020.

Huang, X. and Belongie, S. Arbitrary style transfer in real-time with adaptive instance normalization. In *Proceedings of the IEEE international conference on computer vision*, pp. 1501–1510, 2017.

Ioffe, S. and Szegedy, C. Batch normalization: Accelerating deep network training by reducing internal covariate shift. In *International conference on machine learning*, pp. 448–456. pmlr, 2015.

Jumper, J., Evans, R., Pritzel, A., Green, T., Figurnov, M., Ronneberger, O., Tunyasuvunakool, K., Bates, R., Žídek, A., Potapenko, A., et al. Highly accurate protein structure prediction with alphafold. *Nature*, 596(7873):583–589, 2021.

Karras, T., Laine, S., and Aila, T. A style-based generator architecture for generative adversarial networks. In *Proceedings of the IEEE/CVF conference on computer vision and pattern recognition*, pp. 4401–4410, 2019.

Kipf, T. N. and Welling, M. Semi-supervised classification with graph convolutional networks. In *ICLR*, 2017.

Larsen, R. J. and Marx, M. L. *An introduction to mathematical statistics*. Prentice Hall Hoboken, NJ, 2005.

Li, G., Xiong, C., Thabet, A., and Ghanem, B. Deepgcn: All you need to train deeper gcn, 2020.

Maron, H., Ben-Hamu, H., Serviansky, H., and Lipman, Y. Provably powerful graph networks. In *NeurIPS*, 2019.

Morris, C., Ritzert, M., Fey, M., Hamilton, W. L., Lenssen, J. E., Rattan, G., and Grohe, M. Weisfeiler and leman go neural: Higher-order graph neural networks. In *Proceedings of the AAAI conference on artificial intelligence*, volume 33, 2019.

Morris, C., Kriege, N. M., Bause, F., Kersting, K., Mutzel, P., and Neumann, M. Tudataset: A collection of benchmark datasets for learning with graphs. In *ICML 2020 Workshop on Graph Representation Learning and Beyond (GRL+ 2020)*, 2020.

Morris, C., Lipman, Y., Maron, H., Rieck, B., Kriege, N. M., Grohe, M., Fey, M., and Borgwardt, K. Weisfeiler and leman go machine learning: The story so far. *arXiv preprint arXiv:2112.09992*, 2021.

Murphy, R., Srinivasan, B., Rao, V., and Ribeiro, B. Relational pooling for graph representations. In *International Conference on Machine Learning*, pp. 4663–4673. PMLR, 2019.

Newman, M. *Networks: An Introduction*. Oxford university press, 2010.

Nt, H. and Maehara, T. Revisiting graph neural networks: All we have is low-pass filters. *arXiv preprint arXiv:1905.09550*, 2019.

Ogasawara, E., Martinez, L. C., De Oliveira, D., Zimbrão, G., Pappa, G. L., and Mattoso, M. Adaptive normalization: A novel data normalization approach for non-stationary time series. In *The 2010 International Joint Conference on Neural Networks (IJCNN)*, pp. 1–8. IEEE, 2010.

Park, T., Liu, M.-Y., Wang, T.-C., and Zhu, J.-Y. Semantic image synthesis with spatially-adaptive normalization. In *Proceedings of the IEEE/CVF conference on computer vision and pattern recognition*, pp. 2337–2346, 2019.

Passalis, N., Tefas, A., Kanniainen, J., Gabbouj, M., and Iosifidis, A. Deep adaptive input normalization for time series forecasting. *IEEE transactions on neural networks and learning systems*, 31(9):3760–3765, 2019.

Paszke, A., Gross, S., Massa, F., Lerer, A., Bradbury, J., Chanan, G., Killeen, T., Lin, Z., Gimelshein, N., Antiga, L., Desmaison, A., Kopf, A., Yang, E., DeVito, Z., Raison, M., Tejani, A., Chilamkurthy, S., Steiner, B., Fang, L., Bai, J., and Chintala, S. Pytorch: An imperative

style, high-performance deep learning library. In Wallach, H., Larochelle, H., Beygelzimer, A., d'Alché-Buc, F., Fox, E., and Garnett, R. (eds.), *Advances in Neural Information Processing Systems 32*, pp. 8024–8035. Curran Associates, Inc., 2019.

Puny, O., Ben-Hamu, H., and Lipman, Y. Global attention improves graph networks generalization. *arXiv preprint arXiv:2006.07846*, 2020.

Puny, O., Lim, D., Kiani, B., Maron, H., and Lipman, Y. Equivariant polynomials for graph neural networks. In *International Conference on Machine Learning*, pp. 28191–28222. PMLR, 2023.

Rampášek, L., Galkin, M., Dwivedi, V. P., Luu, A. T., Wolf, G., and Beaini, D. Recipe for a general, powerful, scalable graph transformer. *Advances in Neural Information Processing Systems*, 35:14501–14515, 2022.

Rong, Y., Huang, W., Xu, T., and Huang, J. Dropedge: Towards deep graph convolutional networks on node classification. In *International Conference on Learning Representations*, 2019.

Santurkar, S., Tsipras, D., Ilyas, A., and Madry, A. How does batch normalization help optimization? *Advances in neural information processing systems*, 31, 2018.

Sato, R., Yamada, M., and Kashima, H. Random features strengthen graph neural networks. In *Proceedings of the 2021 SIAM international conference on data mining (SDM)*, pp. 333–341. SIAM, 2021.

Sterling, T. and Irwin, J. J. ZINC 15 – ligand discovery for everyone. *Journal of Chemical Information and Modeling*, 55(11):2324–2337, 11 2015. doi: 10.1021/acs.jcim.5b00559.

Ulyanov, D., Vedaldi, A., and Lempitsky, V. Instance normalization: The missing ingredient for fast stylization. *arXiv preprint arXiv:1607.08022*, 2016.

Vaswani, A., Shazeer, N., Parmar, N., Uszkoreit, J., Jones, L., Gomez, A. N., Kaiser, Ł., and Polosukhin, I. Attention is all you need. *Advances in neural information processing systems*, 30, 2017.

Wang, Y., Sun, Y., Liu, Z., Sarma, S. E., Bronstein, M. M., and Solomon, J. M. Dynamic graph cnn for learning on point clouds. *ACM Transactions on Graphics (tog)*, 38(5):1–12, 2019.

Wu, Y. and He, K. Group normalization. In *Proceedings of the European conference on computer vision (ECCV)*, pp. 3–19, 2018.

Xu, K., Hu, W., Leskovec, J., and Jegelka, S. How powerful are graph neural networks? In *International Conference on Learning Representations*, 2019.

Yang, C., Wang, R., Yao, S., Liu, S., and Abdelzaher, T. Revisiting over-smoothing in deep gcns. *arXiv preprint arXiv:2003.13663*, 2020.

Yehudai, G., Fetaya, E., Meirom, E., Chechik, G., and Maron, H. From local structures to size generalization in graph neural networks. In *International Conference on Machine Learning*, pp. 11975–11986. PMLR, 2021.

Ying, C., Cai, T., Luo, S., Zheng, S., Ke, G., He, D., Shen, Y., and Liu, T.-Y. Do transformers really perform badly for graph representation? *Advances in neural information processing systems*, 34:28877–28888, 2021.

You, J., Gomes-Selman, J. M., Ying, R., and Leskovec, J. Identity-aware graph neural networks. In *Proceedings of the AAAI Conference on Artificial Intelligence*, volume 35, pp. 10737–10745, 2021.

Yun, C., Sra, S., and Jadbabaie, A. Small relu networks are powerful memorizers: a tight analysis of memorization capacity. *Advances in Neural Information Processing Systems*, 32, 2019.

Zhang, B., Feng, G., Du, Y., He, D., and Wang, L. A complete expressiveness hierarchy for subgraph gnns via subgraph weisfeiler-lehman tests. *arXiv preprint arXiv:2302.07090*, 2023a.

Zhang, B., Luo, S., Wang, L., and He, D. Rethinking the expressive power of GNNs via graph biconnectivity. In *The Eleventh International Conference on Learning Representations*, 2023b. URL <https://openreview.net/forum?id=r9hNv76KoT3>.

Zhang, M. and Li, P. Nested graph neural networks. In *Advances in Neural Information Processing Systems*, volume 34, 2021.

Zhao, L. and Akoglu, L. Pairnorm: Tackling oversmoothing in gnns. In *International Conference on Learning Representations*, 2020.

Zhao, L., Jin, W., Akoglu, L., and Shah, N. From stars to subgraphs: Uplifting any GNN with local structure awareness. In *International Conference on Learning Representations*, 2022.

Zhou, K., Huang, X., Li, Y., Zha, D., Chen, R., and Hu, X. Towards deeper graph neural networks with differentiable group normalization. *Advances in neural information processing systems*, 33:4917–4928, 2020.

Zhou, K., Dong, Y., Wang, K., Lee, W. S., Hooi, B., Xu, H., and Feng, J. Understanding and resolving performance degradation in deep graph convolutional networks. In *Proceedings of the 30th ACM International Conference on Information & Knowledge Management*, pp. 2728–2737, 2021.

Zhu, P., Abdal, R., Qin, Y., and Wonka, P. Sean: Image synthesis with semantic region-adaptive normalization. In *Proceedings of the IEEE/CVF Conference on Computer Vision and Pattern Recognition*, pp. 5104–5113, 2020.

## A. Additional Related Work

**Standard Normalization Layers.** BatchNorm (Ioffe & Szegedy, 2015) is arguably one of the most widely used normalization schemes in deep learning. Despite its success, there is little consensus on the exact reason behind the improvements it generally yields. While some studies argue that the effectiveness of BatchNorm lies in its ability to control the problem of internal covariate shift (Ioffe & Szegedy, 2015; Awais et al., 2020), other works (Bjorck et al., 2018; Santurkar et al., 2018) attribute the success to the promotion of faster convergence. Similarly to the other domains, also in graph-learning, BatchNorm normalizes each channel (feature) independently by computing the mean and standard deviation across all the elements in the batch, i.e., across all the nodes in all the graphs in the batch. Another normalization approach that was adopted in graph-learning is InstanceNorm (Ulyanov et al., 2016), which was originally introduced in image style-transfer tasks to remove image-specific contrast and style information. In the context of graphs, InstanceNorm normalizes each channel (feature) independently by computing the mean and standard deviation across all nodes within each graph separately. Additionally, LayerNorm (Ba et al., 2016) was originally proposed for recurrent models, and it is also widely used in Transformers architectures (Vaswani et al., 2017). In the context of graph learning, LayerNorm can take two different versions: Layernorm-node and LayerNorm-graph (Fey & Lenssen, 2019a). The former normalizes each node independently, by computing the mean and standard deviation across all channels within each node separately, while the latter uses the mean and standard deviation across all the channels of all nodes in the entire graph. We visualize these variants in Figure 2. The common theme of these three discussed methods is that they were not originally designed with graph-learning in mind. Next, we discuss graph-designated normalization techniques.

**Graph-Designated Normalization Layers.** PairNorm (Zhao & Akoglu, 2020) was introduced to mitigate the issue of oversmoothing in GNNs, where repeated graph convolutions eventually make node representations indistinguishable from one and the other. The key idea of PairNorm is to ensure that the total pairwise feature distances remain constant across layers, preventing the features of distant nodes from becoming overly similar or indistinguishable. Yang et al. (2020) proposed a different understanding of the oversmoothing issue in GNNs: the authors show that upon initialization GNNs suffer from oversmoothing, but GNNs learn to anti-oversmooth during training. Based on this conclusion, the authors design MeanSubtractionNorm, which removes the mean from the inputs, without rescaling the features. When coupled with GCN (Kipf & Welling, 2017), MeanSubtractionNorm leads to a revised Power Iteration that converges to the Fiedler vector, resulting in a coarse graph partition and faster training. To enhance the performance of GNNs on large graphs, Li et al. (2020) propose MessageNorm, a method that normalizes the aggregated message for each node before combining it with its node features, demonstrating experimental benefits. DiffGroupNorm (Zhou et al., 2020) was designed to alleviate oversmoothing by softly clustering nodes and normalizing nodes within the same group to increase their smoothness while also separating node distributions among different groups. Zhou et al. (2021) explored the impact of transformation operators, such as normalizations, that transform node features after the propagation step in GNNs, and argue that they tend to amplify node-wise feature variance. This effect is shown to lead to performance drop in deep GNNs. To mitigate this issue, they introduced NodeNorm, which scales the feature vector of each node by a root of the standard deviation of its features. This approach also shares similarities with LayerNorm-node. While the aforementioned normalization techniques have made significant strides in mitigating the oversmoothing phenomenon in GNNs, other normalization methods have been proposed to address problems beyond this specific concern. Cai et al. (2021) showed that InstanceNorm serves as a preconditioner for GNNs, thus accelerating their training convergence. However, it also provably degrades the expressiveness of the GNNs for regular graphs. To address this issue, they propose GraphNorm, which builds on top of InstanceNorm by adding a learnable multiplicative factor to the mean for each channel. GraphSizeNorm (Dwivedi et al., 2023) was proposed based on promising empirical results, and aims at normalizing the node features by dividing them by the graph size, before applying a standard BatchNorm layer. UnityNorm (Chen et al., 2022) was introduced to learn graph normalization by optimizing a weighted combination of existing techniques, including LayerNorm-node, InstanceNorm, and BatchNorm. Finally, SuperNorm (Chen et al., 2023) first computes subgraph-specific factors, encompassing the number of nodes and the eigenvalues of the neighborhood-induced subgraph for each node. These subgraph-specific factors are then explicitly embedded at the beginning and end of a standard BatchNorm layer. This approach ensures that any arbitrary GNN layer becomes at least as powerful as the 1-WL test, while simultaneously mitigating the oversmoothing issue. We conclude this paragraph by acknowledging the existence of normalization techniques that focus on normalizing the adjacency matrix before the GNN layers. One common example is the symmetric normalization which is used in GCN (Kipf & Welling, 2017) and subsequent works. Despite their wide use, especially on node-level tasks, these normalizations may fail to capture structural information and lead to less expressive architectures. For instance, a common practice of normalizing the adjacency matrix by dividing its rows by the sum of their entries is equivalent to employing a mean aggregator over the neighbors, which has been shown to fail to distinguish certain non-isomorphic nodes (Xu et al., 2019). For this reason, in

this work, we consider only normalization layers applied to node features after every GNN layer.

**AdaIN and StyleGANs.** Adaptive instance normalization (AdaIN) (Huang & Belongie, 2017; Dumoulin et al., 2016; Ghiasi et al., 2017) was originally proposed for real-time arbitrary style transfer. Given a content input and a style input, AdaIN adjusts the mean and variance of the content input to match those of the style input. This allows for the transfer of stylistic features from the style input to the content input in a flexible and efficient manner. Motivated by style-transfer literature, Karras et al. (2019) introduced StyleGANs as a variant of GANs (Goodfellow et al., 2014) which differs in the generator architecture. More precisely, the generator in StyleGANs starts from a learned constant input and adjusts the “style” of the image at each convolution layer based on the latent code through the usage of AdaIN. Similarly to StyleGANs, we adjust node features at every layer through the usage of noise, i.e., random node features, akin to the role played by the latent code in StyleGANs.

**Random Node Features in GNNs.** Random input features were used in the context of GNNs to improve the expressive power of Message Passing Neural Networks (MPNNs) (Murphy et al., 2019; Puny et al., 2020; Abboud et al., 2020; Sato et al., 2021; Dasoulas et al., 2021). Importantly, MPNNs augmented with random node features have been shown to be universal (with high probability) in Puny et al. (2020); Abboud et al. (2020), a result we naturally inherit when GRANOLA defaults to simply utilizing random node features. Notably, despite the universality results, GNNs augmented with RNF do not consistently improve performance on real-world datasets (Eliasof et al., 2023). We show instead that GRANOLA consistently leads to improved performances.

## B. Comparison of Different Normalizations

In this section we present the different normalization techniques that have been specifically proposed for graph data and highlight their connection to standard normalization schemes (i.e., BatchNorm, InstanceNorm, LayerNorm-node, LayerNorm-graph) whenever this is present.

**PairNorm.** PairNorm (Zhao & Akoglu, 2020) first centers node features by subtracting the mean computed per channel across all the nodes in the graph, similarly to InstanceNorm. Then, it scales the centered vector by dividing it by the square root of the mean (computed across nodes) of the norm of each node feature vector, where the norm is computed over the channel dimension. That is, the center operation has equation:

$$\tilde{h}_{b,n,c}^{(\ell),\text{center}} = \tilde{h}_{b,n,c}^{(\ell)} - \mu_{b,n,c},$$

where  $\mu_{b,n,c}$  is as in InstanceNorm (Equation (5a)), while the scale operation can be written as

$$\text{NORM}(\tilde{h}_{b,n,c}^{(\ell)}; \tilde{\mathbf{H}}^{(\ell)}, \ell) = s \cdot \frac{\tilde{h}_{b,n,c}^{(\ell),\text{center}}}{\sqrt{\frac{1}{N} \sum_{n=1}^N \|\tilde{h}_{b,n}^{(\ell),\text{center}}\|_2^2}}, \quad (13)$$

with  $s \in \mathbb{R}$  a hyperparameter and the norm is

$$\|\tilde{h}_{b,n}^{(\ell),\text{center}}\|_2^2 = \sum_{c=1}^C |\tilde{h}_{b,n,c}^{(\ell),\text{center}}|^2.$$

**MeanSubtractionNorm.** MeanSubtractionNorm (Yang et al., 2020) is similar to InstanceNorm, but it simply shifts its input without dividing it by the standard deviation (and without affine parameters). That is

$$\text{NORM}(\tilde{h}_{b,n,c}^{(\ell)}; \tilde{\mathbf{H}}^{(\ell)}, \ell) = \tilde{h}_{b,n,c}^{(\ell)} - \mu_{b,n,c} \quad (14)$$

and  $\mu_{b,n,c}$  as Equation (5a).

**MessageNorm.** MessageNorm (Li et al., 2020) couples normalization with the GNN layer. In particular, it defines the update rule of  $\mathbf{H}^{(\ell)}$  as follows,

$$h_{b,n}^{(\ell)} = \phi \left( \text{MLP} \left( h_{b,n}^{(\ell-1)} + s \|h_{b,n}^{(\ell-1)}\|_2 \frac{\|m_{b,n}^{(\ell-1)}\|_2}{\|m_{b,n}^{(\ell-1)}\|_2} \right) \right) \quad (15)$$

where  $s \in \mathbb{R}$  a hyperparameter and  $m_{b,n}^{(\ell-1)}$  is the message of node  $n \in [N]$  in graph  $b \in [B]$ , which can be defined as

$$\begin{aligned} m_{b,v,u}^{(\ell)} &= \rho^{(\ell)}(h_{b,v}^{(\ell)}, h_{b,u}^{(\ell)}) \\ m_{b,u}^{(\ell)} &= \zeta^{(\ell)}(\{m_{b,u,v}^{(\ell)} | u \in \mathcal{N}_v^b\}) \end{aligned}$$

with  $\rho^{(\ell)}, \zeta^{(\ell)}$  learnable functions such as MLPs and  $\mathcal{N}_v^b$  neighbors of node  $v$  in graph  $b$ .

**DiffGroupNorm.** DiffGroupNorm (Zhou et al., 2020) first softly clusters nodes and the normalizes nodes within the same cluster by means of BatchNorm. That is, for each graph  $b \in [B]$  in the batch, it computes a soft cluster assignment as

$$\mathbf{S}_b^{(\ell)} = \text{softmax}(\tilde{\mathbf{H}}_b^{(\ell)} \mathbf{W}^{(\ell)})$$

where  $\mathbf{W}^{(\ell)} \in \mathbb{R}^{C \times D}$  with  $D \in \mathbb{N}$  the number of clusters, and therefore  $\mathbf{S}_b^{(\ell)} \in \mathbb{R}^{B \times N \times D}$ . Let us denote by  $\mathbf{S}^{(\ell)} \in \mathbb{R}^{B \times N \times D}$  the matrix containing the cluster assignments for all graphs in the batch, where the  $b$ -th row of  $\mathbf{S}^{(\ell)}$  is  $\mathbf{S}_b^{(\ell)}$ . DiffGroupNorm computes a linear combination of the output of BatchNorm applied to each cluster (where the feature is weighted by the assignment value), and adds the result to the input embedding, that is

$$\text{NORM}(\tilde{h}_{b,n,c}^{(\ell)}; \tilde{\mathbf{H}}^{(\ell)}, \ell) = \tilde{h}_{b,n,c}^{(\ell)} + \lambda \sum_{i=1}^D \text{BATCHNORM}(s_{b,n,i}^{(\ell)} \tilde{h}_{b,n,c}^{(\ell)}; \tilde{\mathbf{H}}^{(\ell)}, \ell), \quad (16)$$

where BATCHNORM leverages Equations (4a) and (4b), and  $\lambda \in \mathbb{R}$  is a hyperparameter. Notably, the term  $\tilde{h}_{b,n,c}^{(\ell)}$  in Equation (16) is similar to a skip connection, with the difference lying in the fact that skip connections usually add the output of the previous layer  $\ell - 1$  after the norm instead of the output of the current layer before the norm.

**NodeNorm.** NodeNorm (Zhou et al., 2021) is similar to LayerNorm-node, but it simply divides its input by a root of its standard deviation, without shifting it and without affine parameters:

$$\text{NORM}(\tilde{h}_{b,n,c}^{(\ell)}; \tilde{\mathbf{H}}^{(\ell)}, \ell) = \frac{\tilde{h}_{b,n,c}^{(\ell)}}{\sigma_{b,n,c}^{\frac{1}{p}}} \quad (17)$$

with  $\sigma$  as in Equation (6b) and  $p \in \mathbb{N}$  a hyperparameter.

**GraphNorm.** GraphNorm (Cai et al., 2021) builds upon InstanceNorm by adding an additional learnable parameter  $\alpha^{(\ell)} \in \mathbb{R}^C$  which is the same for all nodes and graphs. The equation can be written as

$$\text{NORM}(\tilde{h}_{b,n,c}^{(\ell)}; \tilde{\mathbf{H}}^{(\ell)}, \ell) = \gamma_c^{(\ell)} \frac{\tilde{h}_{b,n,c}^{(\ell)} - \alpha_c^{(\ell)} \mu_{b,n,c}}{\sigma_{b,n,c}} + \beta_c^{(\ell)}, \quad (18)$$

and  $\mu_{b,n,c}, \sigma_{b,n,c}$  as Equations (5a) and (5b).

**GraphSizeNorm.** GraphSizeNorm (Dwivedi et al., 2023) normalizes the node features by dividing them by the graph size, before applying a standard BatchNorm:

$$\text{NORM}(\tilde{h}_{b,n,c}^{(\ell)}; \tilde{\mathbf{H}}^{(\ell)}, \ell) = \frac{\tilde{h}_{b,n,c}^{(\ell)}}{\sqrt{N}}. \quad (19)$$

**UnityNorm.** UnityNorm (Chen et al., 2022) consists of a weighted combination of four normalization techniques, where the weights  $\lambda_1, \lambda_2, \lambda_3, \lambda_4 \in \mathbb{R}$  are learnable. That is

$$\begin{aligned} \text{NORM}(\tilde{h}_{b,n,c}^{(\ell)}; \tilde{\mathbf{H}}^{(\ell)}, \ell) &= \lambda_1 \text{LAYERNORM-NODE}(\tilde{h}_{b,n,c}^{(\ell)}; \tilde{\mathbf{H}}^{(\ell)}, \ell) + \\ &\quad \lambda_2 \text{ADJACENCYNORM}(\tilde{h}_{b,n,c}^{(\ell)}; \tilde{\mathbf{H}}^{(\ell)}, \ell) + \\ &\quad \lambda_3 \text{INSTANCENORM}(\tilde{h}_{b,n,c}^{(\ell)}; \tilde{\mathbf{H}}^{(\ell)}, \ell) + \\ &\quad \lambda_4 \text{BATCHNORM}(\tilde{h}_{b,n,c}^{(\ell)}; \tilde{\mathbf{H}}^{(\ell)}, \ell) \end{aligned} \quad (20)$$

where LAYERNORM-NODE, INSTANCENORM and BATCHNORM leverage respectively Equations (4a), (4b), (5a), (5b), (6a) and (6b). ADJACENCYNORM computes the statistics for each node across all features of all its neighbors, that is

$$\mu_{b,n,c} = \frac{1}{|\mathcal{N}_n^b|C} \sum_{u \in \mathcal{N}_n^b} \sum_{c=1}^C \tilde{h}_{b,u,c}^{(\ell)}, \quad \sigma_{b,n,c}^2 = \frac{1}{|\mathcal{N}_n^b|C} \sum_{u \in \mathcal{N}_n^b} \sum_{c=1}^C (\tilde{h}_{b,u,c}^{(\ell)} - \mu_{b,n,c})^2.$$

**SuperNorm.** SuperNorm (Chen et al., 2023) embeds subgraph-specific factors into BatchNorm. First, for each node  $n$  in graph  $b$  it extracts the subgraph induced by its neighbors, denoted as  $S_{b,n}$ . Then, it computes the so called subgraph-specific factors for each subgraph, which are the output of an hash function over the number of nodes in the subgraph and its eigenvalues. That is the subgraph-specific factor of  $S_{b,n}$  is

$$\xi(S_{b,n}) = \text{Hash}(\phi(|V_{S_{b,n}}|), \psi(\text{Eig}_{S_{b,n}}))$$

where  $|V_{S_{b,n}}|$  denotes the number of nodes in  $S_{b,n}$  and  $\text{Eig}_{S_{b,n}}$  its eigenvalues, with  $\phi$  and  $\psi$  injective functions.

Subgraph-specific factors for all subgraphs in a graph  $b$  are collected into a vector  $M_b^G \in \mathbb{R}^{N \times 1}$

$$M_b^G = [\xi(S_{b,1}); \xi(S_{b,2}); \dots; \xi(S_{b,N})]$$

which is used to obtain two additional vectors  $M_b^{SN}, M_b^{RC} \in \mathbb{R}^{N \times 1}$  defined as

$$M_b^{SN} = \left[ \frac{\xi(S_{b,1})}{\sum_{n=1}^N \xi(S_{b,n})}; \frac{\xi(S_{b,2})}{\sum_{n=1}^N \xi(S_{b,n})}; \dots; \frac{\xi(S_{b,N})}{\sum_{n=1}^N \xi(S_{b,n})} \right]$$

$$M_b^{RC} = M_b^G \odot M_b^{SN}.$$

where  $\odot$  denotes the element-wise product. Then, the normalization computes the segment average of  $\tilde{\mathbf{H}}_b^{(\ell)}$  for each graph  $b$ , denoted as  $\tilde{\mathbf{H}}_b^{(\ell),\text{segment}} \in \mathbb{R}^{N \times C}$ , where a row  $n$  is defined as

$$\tilde{h}_{b,n}^{(\ell),\text{segment}} = \sum_{n=1}^N \tilde{h}_{b,n}^{(\ell)}.$$

Then, the input  $\tilde{\mathbf{H}}_b^{(\ell)}$  is calibrated by injecting the subgraph-specific factors as well as the graph statistics obtained via  $\tilde{\mathbf{H}}_b^{(\ell),\text{segment}}$ . That is,

$$\tilde{\mathbf{H}}_b^{(\ell),\text{calibration}} = \tilde{\mathbf{H}}_b^{(\ell)} + \mathbf{W}^{(\ell)} \tilde{\mathbf{H}}_b^{(\ell),\text{segment}} \odot (M_b^{RC} \mathbf{1}_C^\top)$$

where  $\mathbf{1}_C \in \{1\}^{C \times 1}$  and  $\mathbf{W}^{(\ell)} = \mathbf{1}_N \mathbf{w}^{(\ell)\top}$  with  $\mathbf{1}_N \in \{1\}^{N \times 1}$  and  $\mathbf{w}^{(\ell)} \in \mathbb{R}^{C \times 1}$  is a learnable parameter. After injecting subgraph-specific factors, the normalization layer performs BatchNorm on the calibration features, that is

$$\tilde{h}_{b,n,c}^{(\ell),\text{CS}} = \text{BATCHNORM}(\tilde{h}_{b,n,c}^{(\ell),\text{calibration}}; \tilde{\mathbf{H}}_b^{(\ell),\text{calibration}})$$

Finally, subgraph-specific factors are embedded after BatchNorm, by computing

$$\mathbf{H}_b^{(\ell)} = \phi \left( \tilde{\mathbf{H}}_b^{(\ell),\text{CS}} \odot (\mathbf{1}_N \gamma^{(\ell)\top} + \mathbb{P}_b^{(\ell)})/2 + \mathbf{1}_N \beta^{(\ell)\top} \right) \quad (21)$$

where  $\gamma^{(\ell)}, \beta^{(\ell)} \in \mathbb{R}^{C \times 1}$  are learnable affine parameters, and  $\mathbb{P}_b^{(\ell)} \in \mathbb{R}^{N \times C}$  is a matrix where each entry is obtained as

$$\mathbb{P}_{b,n,c}^{(\ell)} = (M_{b,n,c}^{RE}) \mathbf{w}_{RE,c}^{(\ell)}$$

where  $\mathbf{w}_{RE}^{(\ell)} \in \mathbb{R}^C$  is a learnable parameter and  $M_b^{RE} \in \mathbb{R}^{N \times C}$  is obtained as

$$M_b^{RE} = \frac{M_b^{RC}}{\sum_{n=1}^N M_{b,n}^{RC}} \mathbf{1}_C^\top.$$

Equation (21) represents the output of SuperNorm, followed by an activation function  $\phi$ .

## C. Additional Motivating Examples

In the following we elaborate on the failure cases of existing normalization layers. Throughout this section, we will assume that all GNN layers are message-passing layers, and, in particular, we focus on the maximally expressive MPNN layers presented in [Morris et al. \(2019\)](#), which have been shown to be as expressive as the 1-WL test. In particular Equation (1) can be rewritten as follows,

$$\tilde{\mathbf{H}}_b^{(\ell)} = \mathbf{H}_b^{(\ell-1)} \mathbf{W}_1^{(\ell-1)} + \mathbf{A}_b \mathbf{H}_b^{(\ell-1)} \mathbf{W}_2^{(\ell-1)}. \quad (22)$$

*Example C.1* (BatchNorm reduces GNN capabilities to compute node degrees). Consider the following task: Given a graph  $G$ , for each node predict its degree. Assume that our batch contains  $B$  graphs, and, for simplicity, assume that they all have the same number of nodes  $N$ .<sup>3</sup> Assuming such graphs do not have initial node features, we follow standard practice ([Xu et al., 2019](#)) and initialize  $\mathbf{H}_b^{(0)}$  for each graph  $b \in [B]$  as a vector of ones, i.e.,  $\mathbf{H}_b^{(0)} = \mathbf{1} \in \mathbb{R}^{N \times 1}$ . The output of the first GNN layer is already the degree of each node, or a function thereof:

$$\mathbf{H}_b^{(1)} = \phi \left( \text{NORM} \left( \mathbf{H}_b^{(0)} \mathbf{W}_1^{(0)} + \mathbf{A}_b \mathbf{H}_b^{(0)} \mathbf{W}_2^{(0)}; \ell \right) \right), \quad (23)$$

where  $\mathbf{W}_1^{(0)} \in \mathbb{R}^{1 \times C}$ ,  $\mathbf{W}_2^{(0)} \in \mathbb{R}^{1 \times C}$ , are learnable weight matrices, and  $C \in \mathbb{N}$  is the hidden feature dimensionality. Note that since the input is one dimensional, all output channels behave identically. We consider the case where  $C = 1$ . Importantly, in our example, we have that  $\mathbf{H}_b^{(0)} \mathbf{W}_1^{(0)}$  is the same for all nodes in all graphs in the batch, because  $\mathbf{H}_b^{(0)}$  and  $\mathbf{W}_1^{(0)}$  are the same for all nodes and graphs. Therefore, the term  $\mathbf{H}_b^{(0)} \mathbf{W}_1^{(0)}$  acts as a bias term in Equation (23). Thus, for each node, the output of the first GNN layer is simply a linear function of the node degree, which is computed by the term  $\mathbf{A}_b \mathbf{H}_b^{(0)}$  in Equation (23). Now, consider the normalization layer NORM applied to the output of this function, and assume for now that there are no affine parameters. First, the BatchNorm normalization layer subtracts the mean computed across all nodes in all graphs, as shown in Equation (4a). For all nodes having an output smaller than the mean, this subtraction returns a negative number, which is zeroed out by the application of the ReLU which follows the normalization. Therefore, assuming no further layers, for these nodes the prediction can only be 0 regardless of the actual degree, and therefore is incorrect. In Figure 1, we provide a concrete example where this limitation occurs.

*Remark C.2* (Deeper networks are also limited). It is important to note that even when the number of layers is greater than one, and assuming  $C = 1$  in all layers, the problem persists, because the analysis can be applied to every subsequent layer's output by simply noticing that subtracting the mean will always zero out features less than the mean.

*Remark C.3* (BN with Affine transformation is also limited). We highlight that the inclusion of learnable affine parameters in BatchNorm, while potentially mitigating the problem during training by means of a large affine parameter  $\beta_c^{(1)}$  that shifts the negative outputs before the ReLU, does not offer a definitive solution. Indeed, it is always possible to construct a test scenario where one graph has nodes with degrees significantly smaller than those seen while training, for which the learned shift  $\beta_c^{(1)}$  is not sufficiently large to make the output of the normalization layer positive.

It is important to mention that the aforementioned example potentially serves as a failure case for other methods that are based on removing the mean  $\mu_{b,n,c}$  as calculated by BatchNorm in Equation (4a). For instance, GraphSizeNorm ([Dwivedi et al., 2023](#)) also suffers from the same issue, as this normalization technique scales the node features by the number of nodes before applying BatchNorm. Furthermore, Example C.1 can be adjusted to induce a failure case for the normalization operation (excluding the skip link) in DiffGroupNorm ([Zhou et al., 2020](#)), which is also based on BatchNorm. This can be achieved by ensuring that a subset of nodes has a degree less than the average within all the clusters to which it is (softly) assigned.

Example C.1 can be easily adapted to represent a failure case for InstanceNorm. The adaptation involves treating the entire batch as a single graph, which can be further refined to avoid having disconnected components by adding a small number of edges connecting them.

*Example C.4* (InstanceNorm reduces GNN capabilities to compute node degree). Consider the following task: Given a graph  $G$ , for each node predict its degree. Assuming the graph does not have initial node features, we follow standard practice ([Xu et al., 2019](#)) and initialize  $\mathbf{H}_b^{(0)} = \mathbf{1} \in \mathbb{R}^{N \times 1}$ . The output of the first GNN layer is already the degree of each node, or a function thereof. Now, consider the normalization layer NORM applied to the output of this function. First, the InstanceNorm

<sup>3</sup>This assumption is included only to simplify the notation, but can be removed without affecting the results.

normalization layer subtracts the mean computed across all nodes within each graph in the batch, as shown in Equation (5a). For all nodes having an output smaller than the mean within their graph, this subtraction returns a negative number, which is zeroed out by the application of the ReLU activation function, applied following the normalization. Therefore, assuming no further layers, for these nodes the prediction can only be 0 regardless of the actual degree, and therefore is incorrect. Similarly to BatchNorm, the inclusion of learnable affine parameters as well as the stacking of additional single-channel layers is not sufficient to solve the problem.

The aforementioned limitation extends directly to other graph-designed normalizations based on InstanceNorm, such as PairNorm and GraphNorm<sup>4</sup> as they also shifts the input in the same way, based on the mean  $\mu_{b,n,c}$  as defined in Equation (5a).

*Example C.5* (LayerNorm-node reduces GNN capabilities to compute node degree). Consider the following task: Given a graph  $G$ , for each node predict its degree. Consider a graph  $G$  consisting of a path of 3 nodes. Assuming the graph does not have initial node features, we initialize  $\mathbf{H}_b^{(0)} = \mathbf{1} \in \mathbb{R}^{N \times 1}$ , with  $b = 0$  as we only have one graph. We will assume that  $\mathbf{W}_1^{(0)} = \mathbf{0}$  (Equation (22)). Therefore, the output of the first GNN layer can be written as:

$$\mathbf{H}_b^{(1)} = \phi \left( \text{NORM} \left( \mathbf{A}_b \mathbf{H}_b^{(0)} \mathbf{W}_2^{(0)}; \ell \right) \right), \quad (24)$$

which, for each node, is a vector having at each entry the degree of the node multiplied by a learnable weight entry. Compare now one of the node having degree  $d \in \mathbb{N}$ , denoted as  $v$  with the node having degree  $2d$ , denoted as  $u$ . Clearly, we have that the vector of node features in  $u$  is equal to two times the vector of node features in  $v$ . Therefore, by subtracting the mean computed across the channel dimension, as per Equation (6a), we obtain

$$h_{b,u,c}^{(1)} = h_{b,v,c}^{(1)}$$

for all  $c \in [C]$ . This implies that it is not possible to then distinguish the degree of these two nodes.

*Remark C.6* (Deeper networks are also limited). It is important to note that even when the number of layers is greater than one, assuming  $\mathbf{W}_1^{(\ell-1)} = \mathbf{0}$  in all GNN layers (Equation (22)), the problem persists. Indeed, in the next layer, both nodes  $v$  and  $u$  will aggregate neighbors having identical features. Therefore the vector of node features in  $u$  will still be equal to two times the vector of node features in  $v$ , a difference that is removed by the subtraction of the mean computed per node.

## D. Proofs

**Proposition D.1** (MPNN with GRANOLA can implement MPNN with RNF). *Let  $f^{\text{norm}}$  be a stacking of MPNN layers interleaved with GRANOLA normalization layers (Equation (10)), followed by activation functions. There exists a choice of hyperparameters and weights such that  $f^{\text{norm}}$  defaults to MPNN + RNF (Abboud et al., 2020).*

*Proof.* We only need to show a choice of hyperparameters and weights that makes an MPNN + GRANOLA default to an MPNN + RNF, which is the model obtained by performing message passing on the input graph where the initial node features are concatenated to RNF.

Since RNF in an MPNN + GRANOLA are introduced in the GRANOLA layer, we choose the first MPNN layer, which precedes any normalization (Equation (1)), to simply repeat its inputs using additional channels. In the case of GraphConv layers, this is easily obtained by  $\mathbf{W}_1^{(0)} = (\mathbf{I} \ \mathbf{I})$  and  $\mathbf{W}_2^{(0)} = \mathbf{0}$ , with  $\mathbf{I} \in \{0, 1\}^{C \times C}$ . With these choices,  $\tilde{\mathbf{H}}_b^{(1)}$  in Equation (1) becomes  $\tilde{\mathbf{H}}_b^{(1)} = \mathbf{H}_b^{(0)} \oplus \mathbf{H}_b^{(0)} = \mathbf{X}_b \oplus \mathbf{X}_b$ . Notably, this concatenation is only introduced to make the dimension of  $\tilde{\mathbf{H}}_b^{(1)}$  match the dimension of the concatenation of the initial node features with RNF having the same dimension.

Consider the first GRANOLA layer,  $\ell = 1$ . It is sufficient to set the activation functions inside  $\text{GNN}_{\text{NORM}}^{(1)}$  to be the identity function and to properly set the weights of  $\text{GNN}_{\text{NORM}}^{(1)}$  (Equation (8)) and  $f_1^{(1)}, f_2^{(1)}$  (Equation (9)) such that the normalization layer returns  $\mathbf{H}_b^{(0)} \oplus \mathbf{R}_b^{(1)}$ , with  $\mathbf{R}_b^{(1)} \in \mathbb{R}^{N \times K}$  and  $K$  chosen such that  $K = C$ . For example, if  $\text{GNN}_{\text{NORM}}^{(1)}$  is composed by a single GraphConv layer (Morris et al., 2019) (with an identity activation function), we have

$$\begin{aligned} \mathbf{Z}_b^{(1)} &= (\tilde{\mathbf{H}}_b^{(1)} \oplus \mathbf{R}_b^{(1)}) \mathbf{W}_1^{\text{NORM},(1)} + \mathbf{A}_b (\tilde{\mathbf{H}}_b^{(1)} \oplus \mathbf{R}_b^{(1)}) \mathbf{W}_2^{\text{NORM},(1)} \\ &= (\mathbf{H}_b^{(0)} \oplus \mathbf{H}_b^{(0)} \oplus \mathbf{R}_b^{(1)}) \mathbf{W}_1^{\text{NORM},(1)} + \mathbf{A}_b (\mathbf{H}_b^{(0)} \oplus \mathbf{H}_b^{(0)} \oplus \mathbf{R}_b^{(1)}) \mathbf{W}_2^{\text{NORM},(1)}, \end{aligned}$$

<sup>4</sup>Assuming the learned shift parameter in GraphNorm as not all zeros.

then for  $\text{GNN}_{\text{NORM}}^{(1)}$  is sufficient to choose  $\mathbf{W}_2^{\text{NORM},(1)} = \mathbf{0}$ ,  $\mathbf{W}_1^{\text{NORM},(1)} = \begin{pmatrix} \mathbf{0} & \mathbf{0} \\ \mathbf{I} & \mathbf{0} \\ \mathbf{0} & \mathbf{I} \end{pmatrix}$ , where  $\mathbf{I} \in \{0, 1\}^{C \times C}$  is the identity matrix. For  $f_1^{(1)}, f_2^{(1)}$  its is sufficient to set  $f_1^{(1)}$  to always return a zero vector, and  $f_2^{(1)}$  to be the identity function. With these choices, Equation (2) becomes

$$\mathbf{H}^{(1)} = \phi \left( \tilde{\mathbf{H}}_b^{(0)} \oplus \mathbf{R}_b^{(1)} \right) = \phi \left( \mathbf{X}_b \oplus \mathbf{R}_b^{(1)} \right),$$

which represents the input of the next GNN layer, and matches the input of an MPNN + RNF. Therefore, we are only left to show that subsequent applications of GRANOLA layers behave as the identity function, since the GNN layers will instead behave as those in the MPNN + RNF.

After the first GRANOLA layer,  $\ell > 1$ , it is sufficient to set  $\text{GNN}_{\text{NORM}}^{(\ell)}$  (Equation (8)) and  $f_1^{(\ell)}, f_2^{(\ell)}$  (Equation (9)) to return its input  $\tilde{\mathbf{H}}^{(\ell)} \in \mathbb{R}^{N \times C}$  (while discarding  $\mathbf{R}_b^{(\ell)} \in \mathbb{R}^{N \times K}$ ). Assuming a single layer in it (with an identity activation function), this can be accomplished by setting  $\mathbf{W}_2^{\text{NORM},(\ell)} = \mathbf{0}$  and  $\mathbf{W}_1^{\text{NORM},(\ell)} = \begin{pmatrix} \mathbf{I} & \mathbf{0} \\ \mathbf{0} & \mathbf{I} \end{pmatrix}$ ,  $f_1^{(\ell)}$  to always return a zero vector, and  $f_2^{(\ell)}$  to be the identity function. With these choices, Equation (10) becomes

$$\text{NORM}(\tilde{h}_{b,n,c}^{(\ell)}; \tilde{\mathbf{H}}^{(\ell)}, \ell) = \tilde{h}_{b,n,c}^{(\ell)}.$$

Therefore, these two steps imply that an MPNN with GRANOLA implements an MPNN with RNF.  $\square$

**Corollary D.2** (MPNN + GRANOLA is universal with high probability). *Let  $\Omega_N$  be a compact set of graphs with  $N \in \mathbb{N}$  nodes and  $g$  a continuous permutation-invariant graph function defined over  $\Omega_N$ . Let  $f^{\text{norm}}$  be a stacking of MPNN layers interleaved with GRANOLA normalization layers (Equation (10)) followed by activation functions. Then, if random node features inside GRANOLA are sampled from a continuous bounded distribution with zero mean and finite variance, for all  $\epsilon, \delta > 0$ , there exist a choice of hyperparameters and weights such that,  $\forall G = (\mathbf{A}, \mathbf{X}) \in \Omega$ ,*

$$P(|g(\mathbf{A}, \mathbf{X}) - f^{\text{norm}}(\mathbf{A}, \mathbf{X})| \leq \epsilon) \geq 1 - \delta \quad (25)$$

where  $f^{\text{norm}}(\mathbf{A}, \mathbf{X})$  is the output for the considered choice of hyperparameters and weights.

*Proof.* The proof follows by showing the choice of hyperparameters and weights which makes an MPNN augmented with GRANOLA satisfy the assumptions of Puny et al. (2020, Proposition 1). In all our GRANOLA layers,  $\mathbf{R}_b^{(\ell)} \in \mathbb{R}_b^{N \times K}$  is drawn from a continuous and bounded distribution for any graph  $b$  in a batch of  $B$  graphs. Therefore, we only need to show that the overall architecture can default to an MPNN augmented with these RNF. This follows from Proposition D.1.  $\square$

**Proposition 4.1** (RNF are necessary in GRANOLA for increased expressive power). *Let  $N$  be a natural number and consider all graphs of size  $N$ . An MPNN with GRANOLA-NO-RNF (Equation (12)) is not more expressive than a standard MPNN.*

*Proof.* The proof follows by showing that an MPNN with GRANOLA-NO-RNF can be implemented by a standard MPNN (without any normalization), which therefore represents an upper-bound of its expressive power.

We assume that all the MPNN layers are maximally expressive MPNNs layers of the form of GraphConv (Morris et al., 2019), and that all activation functions inside GRANOLA-NO-RNF are ReLU activation functions. Since the convolution layers are the same in both  $f^{\text{norm}}$  and  $f$ , we are only left to show that an MPNN (without normalization, with ReLU activations) can implement a layer of GRANOLA-NO-RNF. Recall that a single GRANOLA layer can be written as

$$\text{NORM}(\tilde{h}_{b,n,c}^{(\ell)}; \tilde{\mathbf{H}}^{(\ell)}, \ell) = f_1^{(\ell)}(z_{b,n}^{(\ell)})_c \frac{\tilde{h}_{b,n,c}^{(\ell)} - \mu_{b,n,c}}{\sigma_{b,n,c}} + f_2^{(\ell)}(z_{b,n}^{(\ell)})_c, \quad (26)$$

and, since we are not considering RNF,  $\mathbf{Z}_b^{(\ell)}$  is obtained with Equation (12), recalling that  $\text{GNN}_{\text{NORM}}^{(\ell)}$  is also composed by MPNN layers interleaved by ReLU activation functions per our assumption. We denote the number of layers of this GNN by  $L_{\text{NORM}}^{(\ell)}$ . We next show how to obtain Equation (26) using multiple layers of an MPNN which takes as input  $\tilde{\mathbf{H}}^{(\ell)}$ . We will denote intermediate layers of this MPNN as  $\tilde{\mathbf{H}}^{(t)}$ ,  $t \geq 1$ .

**First Step, compute  $\mathbf{Z}_b^{(\ell)}$ .** The first layers of this MPNN are used to obtain  $\mathbf{Z}_b^{(\ell)}$  given  $\tilde{\mathbf{H}}_b^{(\ell)}$ , effectively mimicking  $\text{GNN}_{\text{NORM}}^{(\ell)}$ . Since we will later need also  $\tilde{\mathbf{H}}_b^{(\ell)}$ , we will use the last feature dimensions in every layer representation to simply

copy it in every subsequent layer. Importantly, however, simply copying  $\tilde{\mathbf{H}}_b^{(\ell)}$  in the last dimensions using an identity weight matrix may not be sufficient, as the application of ReLU non-linearity would clip negative entries to 0. Therefore, we copy both  $\tilde{\mathbf{H}}_b^{(\ell)}$  and  $-\tilde{\mathbf{H}}_b^{(\ell)}$  in the last dimensions, and at the end recover  $\tilde{\mathbf{H}}_b^{(\ell)}$  as  $\tilde{\mathbf{H}}_b^{(\ell)} = \phi(\tilde{\mathbf{H}}_b^{(\ell)}) - \phi(-\tilde{\mathbf{H}}_b^{(\ell)})$ , with  $\phi$  the ReLU activation.

For  $t = 1$ , the MPNN layer is simply responsible of replicating its input  $\tilde{\mathbf{H}}_b^{(\ell)}$ , so that we can later use the first  $C$  channels to obtain  $\mathbf{Z}_b^{(\ell)}$  and the last to later recover  $\tilde{\mathbf{H}}_b^{(\ell)}$ . Therefore,

$$\hat{\mathbf{H}}_b^{(1)} = \phi(\tilde{\mathbf{H}}_b^{(\ell)} \hat{\mathbf{W}}_1^{(1)} + \mathbf{A}_b \tilde{\mathbf{H}}_b^{(\ell)} \hat{\mathbf{W}}_2^{(1)})$$

with  $\hat{\mathbf{W}}_1^{(1)} = (\mathbf{I} \ \mathbf{I} \ -\mathbf{I})$  and  $\hat{\mathbf{W}}_2^{(1)} = \mathbf{0}$ , with  $\mathbf{I} \in \{0, 1\}^{C \times C}$  the identity matrix, and  $\phi$  is the identity activation function. This means that  $\hat{\mathbf{H}}_b^{(1)} = \tilde{\mathbf{H}}_b^{(\ell)} \oplus \tilde{\mathbf{H}}_b^{(\ell)} \oplus -\tilde{\mathbf{H}}_b^{(\ell)}$ . For  $t > 1$  and  $t \leq L_{\text{NORM}}^{(\ell)} + 1$ , we need to mimic  $\text{GNN}_{\text{NORM}}^{(\ell)}$  from Equation (12) on the first  $C$  dimensions. This is achievable by

$$\hat{\mathbf{H}}_b^{(t+1)} = \phi(\hat{\mathbf{H}}_b^{(t)} \hat{\mathbf{W}}_1^{(t)} + \mathbf{A}_b \hat{\mathbf{H}}_b^{(t)} \hat{\mathbf{W}}_2^{(t)})$$

with  $\hat{\mathbf{W}}_1^{(t)} = \begin{pmatrix} \mathbf{W}_1^{\text{NORM},(t)} & \mathbf{0} & \mathbf{0} \\ \mathbf{0} & \mathbf{I} & \mathbf{0} \\ \mathbf{0} & \mathbf{0} & \mathbf{I} \end{pmatrix}$  and  $\hat{\mathbf{W}}_2^{(t)} = \begin{pmatrix} \mathbf{W}_2^{\text{NORM},(t)} & \mathbf{0} & \mathbf{0} \\ \mathbf{0} & \mathbf{I} & \mathbf{0} \\ \mathbf{0} & \mathbf{0} & \mathbf{I} \end{pmatrix}$ , where  $\mathbf{W}_1^{\text{NORM},(t)}, \mathbf{W}_2^{\text{NORM},(t)}$  are exactly the same as the corresponding weights of  $\text{GNN}_{\text{NORM}}^{(\ell)}$ ,  $\phi$  is the ReLU activation. Therefore, after  $L_{\text{NORM}}^{(\ell)} + 1$  layers, we have

$$\hat{\mathbf{H}}_b^{(L_{\text{NORM}}^{(\ell)} + 1)} = \mathbf{Z}_b^{(\ell)} \oplus \phi(\tilde{\mathbf{H}}_b^{(\ell)}) \oplus \phi(-\tilde{\mathbf{H}}_b^{(\ell)})$$

We can then use an additional MPNN layer  $t$  to recover  $\tilde{\mathbf{H}}_b^{(\ell)}$  by setting  $\hat{\mathbf{W}}_1^{(t)} = \begin{pmatrix} \mathbf{I} & \mathbf{0} \\ \mathbf{0} & \mathbf{I} \\ \mathbf{0} & -\mathbf{I} \end{pmatrix}$ ,  $\hat{\mathbf{W}}_2^{(t)} = \mathbf{0}$ , and obtain

$$\hat{\mathbf{H}}_b^{(L_{\text{NORM}}^{(\ell)} + 2)} = \mathbf{Z}_b^{(\ell)} \oplus \tilde{\mathbf{H}}_b^{(\ell)}$$

Finally, we rely on the ability of MLPs to memorize a finite number of input-output pairs (see [Yun et al. \(2019\)](#) and [Yehudai et al. \(2021, Lemma B.2\)](#)) to implement Equation (26) given its input. This is achieved by making the three subsequent layers of the MPNN behave as a 3-layer MLP (with ReLU activations) by simply zeroing out  $\hat{\mathbf{W}}_2^{(t)}$ . In this way, we have obtained Equation (26) through MPNN layers only.  $\square$

## E. Experimental Details

We implemented GRANOLA using Pytorch ([Paszke et al., 2019](#)) and Pytorch-Geometric ([Fey & Lenssen, 2019b](#)). We ran our experiments on NVIDIA RTX3090 and RTX4090 GPUs, both having 24GB of memory. We performed hyperparameter tuning using the Weight and Biases framework ([Biewald, 2020](#)). To sample the random node features, we followed [Abboud et al. \(2020\)](#) and used a standard Gaussian with mean 0 and variance 1. For each node, we sample independently a number of random features equal to the channel dimension of  $\tilde{h}_{b,n}^{(\ell)}$ , that is  $K$  is equal to  $C$  in Equation (8). Recall that when augmenting a GNN architecture with GRANOLA, we have two types of networks: (i) the main downstream network, and (ii) the normalization network returning  $\mathbf{Z}_b^{(\ell)}$  (see Equation (8)). In both networks, and throughout all datasets that do not contain edge features (e.g., in TUDatasets), we employ GIN layers ([Xu et al., 2019](#)) to perform message passing. In case edge features are available, such as in ZINC, we use the GINE variant of GIN, as prescribed in [Dwivedi et al. \(2023\)](#). For brevity, we refer to both as GIN throughout the paper. Our MLPs are composed of two linear layers with ReLU non-linearities. Our normalization network is kept small and comprises a number of layers tuned in  $\{1, 2, 3\}$  and an embedding dimension that is the same as its input  $\tilde{\mathbf{H}}^{(\ell)}$ . Each experiment is repeated for 5 different seeds, and we report the average and standard deviation result. Details of hyperparameter grid for each dataset can be found in the following subsections.

### E.1. ZINC-12k

We consider the dataset splits proposed in [Dwivedi et al. \(2023\)](#), and use the Mean Absolute Error (MAE) both as loss and evaluation metric. For all models, we used a batch size tuned in  $\{32, 64, 128\}$ . To optimize the model we use the Adam optimizer with initial learning rate of 0.001, which is decayed by 0.5 every 300 epochs. The maximum number of epochs is set to 500. The test metric is computed at the best validation epoch. The downstream network is composed of a number of layers in  $\{4, 6\}$ , with an embedding dimension tuned in  $\{32, 64\}$ .

Table 4: Average batch runtimes on a Nvidia RTX-2080 GPU of GRANOLA and other methods, with 8 layers, batch size of 128, and 128 channels on the OGBG-MOLHIV DATASET. For reference, we also include the measured metric, which is ROC-AUC.

Method	Training Time (ms)	MOLHIV	
		Inference Time (ms)	ROC-AUC $\uparrow$
<b>MPNN</b>			
GIN + BatchNorm (Xu et al., 2019)	4.12	3.23	75.58 $\pm$ 1.40
<b>Subgraph GNNs</b>			
DSS-GNN (EGO+) (Bevilacqua et al., 2022)	69.58	49.88	76.78 $\pm$ 1.66
<b>Natural Baselines</b>			
GIN + BatchNorm + RNF-PE (Sato et al., 2021)	5.16	4.54	75.98 $\pm$ 1.63
GIN + RNF-NORM	7.34	5.59	77.61 $\pm$ 1.64
GIN + GRANOLA-NO-RNF	10.82	9.21	77.09 $\pm$ 1.49
GIN + GRANOLA-MS	11.15	9.37	78.84 $\pm$ 1.22
GIN + GRANOLA	11.24	9.55	78.98 $\pm$ 1.17

## E.2. OGB datasets

We consider the scaffold splits proposed in Hu et al. (2020), and for each dataset we used the loss and evaluation metric prescribed therein. In all experiments, we used the Adam optimizer with initial learning rate of 0.001. We tune the batch size in  $\{64, 128\}$ . We employ a learning rate scheduler that follows the procedure prescribed in Bevilacqua et al. (2022). We also consider dropout in between layers with probabilities in  $\{0, 0.5\}$ . The downstream network has the number of layers in  $\{4, 6\}$  with embedding dimensions in  $\{32, 64, 128\}$ . The maximum number of epochs is set to 500 for all models. The test metric is computed at the best validation epoch.

## E.3. TUDatasets

For all the experiments with datasets from the TUDatasets repository, we followed the evaluation procedure proposed in Xu et al. (2019), consisting of 10-fold cross validation and metric at the best averaged validation accuracy across the folds. The downstream network is composed of a number of layers tuned in  $\{4, 6\}$  layers with embedding dimension in  $\{32, 64\}$ . We use the Adam optimizer with learning rate tuned in  $\{0.01, 0.001\}$ . We consider batch size in  $\{32, 64, 128\}$ , and trained for 500 epochs.

## F. Complexity and Runtimes

**Complexity.** As described in Section 3, and specifically in Equation (10), our GRANOLA takes random node feature and hidden learned node features, and propagates them using a GNN backbone denoted by  $\text{GNN}_{\text{NORM}}$  to compute intermediate (expressive) features, which are then used to calculate the normalization statistics, as shown in Equation (9). The calculation can be implemented either by considering their mean and standard-deviation, as in GRANOLA-MS, or more generally by employing an MLP in GRANOLA, as described in Equations (11a) and (11b) and Equation (9), respectively. In our experiments,  $\text{GNN}_{\text{NORM}}^{(\ell)}$  in GRANOLA is also an MPNN, similar to the downstream backbone model. Therefore, including our GRANOLA layers does not change the asymptotic computational complexity of the architecture, which remains within the computational complexity of MPNNs (e.g., Morris et al. (2019); Xu et al. (2019)). Specifically, each MPNN layer is linear in the number of nodes  $|V|$  and edges  $|E|$ . Since a single GRANOLA layer is composed by  $L_{\text{NORM}}^{(\ell)}$  MPNN layers, assuming it the same for all  $\ell$ , it has a time complexity of  $\mathcal{O}(L_{\text{NORM}} \cdot (|V| + |E|))$ . Every downstream MPNN layer in our framework uses a GRANOLA normalization layer, and therefore, assuming  $L$  downstream MPNN layers, the overall complexity of an MPNN augmented with GRANOLA is  $\mathcal{O}((L \cdot L_{\text{NORM}}) \cdot (|V| + |E|))$ , compared to the complexity of an MPNN without GRANOLA which amounts to  $\mathcal{O}(L \cdot (|V| + |E|))$ . In practice,  $L_{\text{NORM}}$  is a hyperparameter between 1 to 3 and can therefore be considered a constant.

**Runtimes.** While the asymptotic complexity remains linear with respect to the number of nodes and edges in the graph, as in standard MPNNs, our GRANOLA requires some additional computations due to the hidden layers in the normalization mechanism. To measure the impact of these additional layers, we measure the required training and inference times of

Table 5: Ablation study of RNF-PE with GIN and various normalization methods.

Method	ZINC MAE ↓	MOLHIV ROC-AUC ↑
GIN + BatchNorm (Xu et al., 2019)	0.1630±0.04	75.58±1.40
GIN + BatchNorm + RNF-PE (Sato et al., 2021)	0.1621±0.014	75.98±1.63
GIN + LayerNorm-node + RNF-PE	0.1663±0.015	76.22±1.58
GIN + LayerNorm-graph + RNF-PE	0.1624±0.018	76.49±1.64
GIN + Identity + RNF-PE	0.2063±0.018	75.31±2.04
GRANOLA	0.1203±0.006	78.98±1.17

 Table 6: Ablation study of the depth (number of layers) of  $\text{GNN}_{\text{NORM}}^{(\ell)}$ 

Depth	0 (Equiv. to RNF-NORM)	1	2	3	4
ZINC (MAE ↓)	0.1562±0.013	0.1218±0.009	0.1203±0.006	0.1209±0.010	0.1224±0.008
MOLHIV (ROC-AUC ↑)	77.61±1.64	78.33±1.34	78.98±1.17	78.86±1.20	78.21±1.31

GRANOLA, whose results are reported in Table 4. Specifically, we report the average time per batch measured on a Nvidia RTX-2080 GPU. For a fair comparison, in all methods, we use the same number of layers, batch size and number of channels. Our results indicate that while GRANOLA requires additional computational time, it is still a fraction of the cost of more complex methods like Subgraph GNNs, while yielding favorable downstream performance.

## G. Additional Experimental Results

### G.1. RNF as PE Ablation Study

GRANOLA benefits from (i) enhanced expressiveness, and (ii) graph adaptivity. Property (i) is obtained by augmenting our normalization scheme with RNF, as shown in Figure 3. Therefore, it is important to ensure that the contribution GRANOLA does not stem solely from the use of RNF, but rather the overall approach and design of our method.

To this end, in addition to the natural baseline of RNF-PE, which uses RNF as positional encoding combined with GIN + BatchNorm (as in (Sato et al., 2021)), we now provide results of RNF-PE when combined with GIN and different normalization layers. Specifically, we consider Identity (no normalization) and LayerNorm (both graph and node variants). The results are provided in Table 5, together with the results of our GRANOLA, for reference and convenience of comparison. The results suggest that while the different variants of RNF-PE do not show significant improvement over the baseline of GIN + BatchNorm, our GRANOLA does. These results are further evidence that while RNF are theoretically powerful, they may not be significant in practice, as shown in Eliasof et al. (2023). Instead, it is important to incorporate them in a thoughtful manner, for example, to obtain graph adaptivity within the normalization layer, as in our GRANOLA.

### G.2. $\text{GNN}_{\text{NORM}}^{(\ell)}$ Depth Ablation Study

As discussed in Section 3, our GRANOLA utilizes a GNN to learn graph-adaptive normalization shift and scaling parameters, and we denote this GNN by  $\text{GNN}_{\text{NORM}}^{(\ell)}$ . Combined with the RNF as part of the input to  $\text{GNN}_{\text{NORM}}^{(\ell)}$ , we are able to obtain both enhanced expressiveness (from RNF) and graph-adaptivity (by  $\text{GNN}_{\text{NORM}}^{(\ell)}$ ). It is therefore interesting to study the effect of the number of layer in  $\text{GNN}_{\text{NORM}}^{(\ell)}$  on the downstream performance. Specifically, in the case where  $\text{GNN}_{\text{NORM}}^{(\ell)}$  has 0 layers, the experiment defaults to the RNF-NORM baseline, meaning that we use only RNF to determine the normalization parameters, thereby losing graph adaptivity. In Table 6 we provide results on varying number of layers, from 0 to 4. Our results suggest that there is a significant importance in terms of performance to having graph adaptivity in the normalization technique, as offered by our GRANOLA.

### G.3. Combining GRANOLA with Expressive Methods

Table 7: Empirical results with GSN + GRANOLA

Method	ZINC	MOLHIV
	MAE ↓	ROC-AUC ↑
GSN (Bouritsas et al., 2022)	0.1010±0.010	80.39±0.90
GSN + GRANOLA	0.0766±0.008	81.12±0.79

The primary goal of GRANOLA is to rethink the normalization scheme of MPNNs. As such, our experiments focus on studying the theoretical and empirical benefit of augmenting standard MPNNs such as GIN (Xu et al., 2019) with GRANOLA. However, it is also interesting to understand whether expressive, domain-expert guided approaches such as GSN (Bouritsas et al., 2022) can also benefit from GRANOLA. To this end, we augment GSN with GRANOLA, and report the results on ZINC-12K and MOLHIV in Table 7. Our results indicate that in addition to GRANOLA being beneficial for standard MPNNs, it is also useful when combined with more powerful methods like GSN.

#### G.4. Comparison with additional baselines

In the main paper, in Section 5, we focused on providing a comprehensive comparison with directly comparable methods, i.e., standard normalization methods, graph normalization methods, as well as our own set of natural baselines. In this section, we provide additional comparisons with other expressive approaches, such as positional encoding methods and Subgraph GNNs. Our additional comparisons on ZINC-12k, OGB, and TUDatasets are provided in Table 8, Table 9, and Table 10, respectively.

It is important to note, that while some of these methods achieve better performance than our GRANOLA, they are not within the same complexity class as GRANOLA, and specifically they are not linear with respect to the number of nodes and edges in the graph, as discussed in Appendix F. For example, RFP-QR- $\hat{\mathbf{L}}$ ,  $\hat{\mathbf{A}}$ ,  $\mathbf{S}^{\text{learn}}\text{-DSS}$  (Eliasof et al., 2023), which also utilizes the expressive power of RNF, achieves an MAE of 0.1106 on ZINC-12K, while our GRANOLA achieves 0.1203. However, the former is of quadratic complexity with respect to the number of nodes, while GRANOLA is linear, as standard MPNNs. On the other hand, the linear and thus directly comparable RFP -  $\ell_2$  -  $\hat{\mathbf{L}}$ ,  $\hat{\mathbf{A}}$  achieves a higher (worse) MAE of 0.1368. Therefore, we find that our GRANOLA offers a practical yet powerful approach for utilizing RNF.

Additionally, we observe that in some cases, GRANOLA achieves similar or better performance than other expressive and asymptotically more complex methods. For example, our results on TUDatasets in Table 10 show that GRANOLA offers better performance than DSS-GNN (Bevilacqua et al., 2022) on all considered datasets, despite DSS being quadratic in the number of nodes.

Table 8: Additional comparisons of GRANOLA with various baselines on the ZINC-12K graph dataset. All methods obey to the 500k parameter budget.

Method	ZINC (MAE $\downarrow$ )
<b>MPNNs</b>	
GCN (Kipf & Welling, 2017)	0.321 $\pm$ 0.009
PNA (Corso et al., 2020)	0.133 $\pm$ 0.011
<b>POSITIONAL ENCODING METHODS</b>	
GIN + Laplacian PE (Eliasof et al., 2023)	0.1557 $\pm$ 0.012
RFP - $\ell_2$ - $\hat{L}$ , $\hat{A}$ (Eliasof et al., 2023)	0.1368 $\pm$ 0.010
RWPE (Dwivedi et al., 2022)	0.1279 $\pm$ 0.005
RFP-QR- $\hat{L}$ , $\hat{A}$ , $\mathbf{S}^{\text{learn}}$ -DSS (Eliasof et al., 2023)	0.1106 $\pm$ 0.012
<b>DOMAIN-AWARE GNNs</b>	
GSN (Bouritsas et al., 2022)	0.101 $\pm$ 0.010
CIN (Bodnar et al., 2021a)	0.079 $\pm$ 0.006
<b>HIGHER ORDER GNNs</b>	
PPGN (Maron et al., 2019)	0.079 $\pm$ 0.005
PPGN++ (6) (Puny et al., 2023)	0.071 $\pm$ 0.001
<b>GRAPH TRANSFORMERS</b>	
GPS (Rampášek et al., 2022)	0.070 $\pm$ 0.004
GRAPHORMER (Ying et al., 2021)	0.122 $\pm$ 0.006
GRAPHORMER-GD (Zhang et al., 2023b)	0.081 $\pm$ 0.009
<b>SUBGRAPH GNNs</b>	
NGNN (Zhang & Li, 2021)	0.111 $\pm$ 0.003
DS-GNN (EGO+) (Bevilacqua et al., 2022)	0.105 $\pm$ 0.003
DSS-GNN (EGO+) (Bevilacqua et al., 2022)	0.097 $\pm$ 0.006
GNN-AK (Zhao et al., 2022)	0.105 $\pm$ 0.010
GNN-AK+ (Zhao et al., 2022)	0.091 $\pm$ 0.011
SUN (EGO+) (Frasca et al., 2022)	0.084 $\pm$ 0.002
GNN-SSWL (Zhang et al., 2023a)	0.082 $\pm$ 0.003
GNN-SSWL+ (Zhang et al., 2023a)	0.070 $\pm$ 0.005
DS-GNN (NM) (Bevilacqua et al., 2023)	0.087 $\pm$ 0.003
<b>NATURAL BASELINES</b>	
GIN + BatchNorm + RNF-PE (Sato et al., 2021)	0.1621 $\pm$ 0.014
GIN + RNF-NORM	0.1562 $\pm$ 0.013
<b>STANDARD NORMALIZATION LAYERS</b>	
GIN + BatchNorm (Xu et al., 2019)	0.1630 $\pm$ 0.004
GIN + InstanceNorm (Ulyanov et al., 2016)	0.2984 $\pm$ 0.017
GIN + LayerNorm-node (Ba et al., 2016)	0.1649 $\pm$ 0.009
GIN + LayerNorm-graph (Ba et al., 2016)	0.1609 $\pm$ 0.014
GIN + Identity	0.2209 $\pm$ 0.018
<b>GRAPH NORMALIZATION LAYERS</b>	
GIN + PairNorm (Zhao & Akoglu, 2020)	0.3519 $\pm$ 0.008
GIN + MeanSubtractionNorm (Yang et al., 2020)	0.1632 $\pm$ 0.021
GIN + DiffGroupNorm (Zhou et al., 2020)	0.2705 $\pm$ 0.024
GIN + NodeNorm (Zhou et al., 2021)	0.2119 $\pm$ 0.017
GIN + GraphNorm (Cai et al., 2021)	0.3104 $\pm$ 0.012
GIN + GraphSizeNorm (Dwivedi et al., 2023)	0.1931 $\pm$ 0.016
GIN + SuperNorm (Chen et al., 2023)	0.1574 $\pm$ 0.018
GIN + GRANOLA-NO-RNF	0.1497 $\pm$ 0.008
GIN + GRANOLA-MS	0.1238 $\pm$ 0.009
GIN + GRANOLA	0.1203 $\pm$ 0.006

Table 9: Additional comparisons of GRANOLA to natural baselines, standard and graph normalization layers, and subgraph GNNs, demonstrating the practical advantages of our approach. – indicates the results was not reported in the original paper.

Method ↓ / Dataset →	MOLESOL RMSE ↓	MOLTOX21 ROC-AUC ↑	MOLBACE ROC-AUC ↑	MOLHIV ROC-AUC ↑
<b>MPNNs</b>				
GCN (Kipf & Welling, 2017)	1.114±0.036	75.29±0.69	79.15±1.44	76.06±0.97
GIN (Xu et al., 2019)	1.173±0.057	74.91±0.51	72.97±4.00	75.58±1.40
<b>POSITIONAL ENCODING METHODS</b>				
GIN + Laplacian PE (Eliasof et al., 2023)	–	–	–	77.88±1.82
RFP - $\ell_2$ - $\hat{\mathbf{L}}$ , $\hat{\mathbf{A}}$ (Eliasof et al., 2023)	–	–	–	77.91±1.43
RWPE (Dwivedi et al., 2022)	–	–	–	78.62±1.13
RFP-QR- $\hat{\mathbf{L}}$ , $\hat{\mathbf{A}}$ , $\mathbf{S}^{\text{learn}}$ -DSS (Eliasof et al., 2023)	–	–	–	80.58±1.21
<b>EXPRESSIVE GNNs</b>				
GSN (Bouritsas et al., 2022)	–	–	–	80.39±0.90
CIN (Bodnar et al., 2021a)	–	–	–	80.94±0.57
<b>SUBGRAPH GNNs</b>				
RECONSTR. GNN (Cotta et al., 2021)	1.026±0.033	75.15±1.40	–	76.32±1.40
NGNN (Zhang & Li, 2021)	–	–	–	78.34±1.86
DS-GNN (EGO+) (Bevilacqua et al., 2022)	–	76.39±1.18	–	77.40±2.19
DSS-GNN (EGO+) (Bevilacqua et al., 2022)	–	77.95±0.40	–	76.78±1.66
GNN-AK+ (Zhao et al., 2022)	–	–	–	79.61±1.19
SUN (GIN) (EGO+) (Frasca et al., 2022)	–	–	–	80.03±0.55
GNN-SSWL+ (Zhang et al., 2023a)	–	–	–	79.58±0.35
DS-GNN (NM) (Bevilacqua et al., 2023)	0.847±0.015	76.25±1.12	78.41±1.94	76.54±1.37
<b>NATURAL BASELINES</b>				
GIN + BatchNorm + RNF-PE (Sato et al., 2021)	1.052±0.041	75.14±0.67	74.28±3.80	75.98±1.63
GIN + RNF-NORM	1.039±0.040	75.12±0.92	77.96±4.36	77.61±1.64
<b>STANDARD NORMALIZATION LAYERS</b>				
GIN + BatchNorm (Xu et al., 2019)	1.173±0.057	74.91±0.51	72.97±4.00	75.58±1.40
GIN + InstanceNorm (Ulyanov et al., 2016)	1.099±0.038	73.82±0.96	74.86±3.37	76.88±1.93
GIN + LayerNorm-node (Ba et al., 2016)	1.058±0.024	74.81±0.44	77.12±2.70	75.24±1.71
GIN + LayerNorm-graph (Ba et al., 2016)	1.061±0.043	75.03±1.24	76.49±4.07	76.13±1.84
GIN + Identity	1.164±0.059	73.34±1.08	72.55±2.98	71.89±1.32
<b>GRAPH NORMALIZATION LAYERS</b>				
GIN + PairNorm (Zhao & Akoglu, 2020)	1.084±0.031	73.27±1.05	75.11±4.24	76.18±1.47
GIN + MeanSubtractionNorm (Yang et al., 2020)	1.062±0.045	74.98±0.62	76.36±4.47	76.37±1.40
GIN + DiffGroupNorm (Zhou et al., 2020)	1.087±0.063	74.48±0.76	75.96±3.79	74.37±1.68
GIN + NodeNorm (Zhou et al., 2021)	1.068±0.029	73.27±0.83	75.67±4.03	75.50±1.32
GIN + GraphNorm (Cai et al., 2021)	1.044±0.027	73.54±0.80	73.23±3.88	78.08±1.16
GIN + GraphSizeNorm (Dwivedi et al., 2023)	1.121±0.051	74.07±0.30	76.18±3.52	75.44±1.51
GIN + SuperNorm (Chen et al., 2023)	1.037±0.044	75.08±0.98	75.12±3.38	76.55±1.76
GIN + GRANOLA-NO-RNF	1.088±0.032	75.87±0.72	76.23±2.06	77.09±1.49
GIN + GRANOLA-MS	0.971±0.026	77.32±0.67	79.18±2.41	78.84±1.22
GIN + GRANOLA	0.960±0.020	77.19±0.85	79.92±2.56	78.98±1.17

Table 10: Additional Graph classification accuracy (%)  $\uparrow$  on TUDatasets. – indicates the results was not reported in the original paper.

Method $\downarrow$ / Dataset $\rightarrow$	MUTAG	PTC	PROTEINS	NCI1	NCI109
<b>EXPRESSIVE GNNs</b>					
GSN (Bouritsas et al., 2022)	92.2 $\pm$ 7.5	68.2 $\pm$ 7.2	76.6 $\pm$ 5.0	83.5 $\pm$ 2.0	–
SIN (Bodnar et al., 2021b)	–	–	76.4 $\pm$ 3.3	82.7 $\pm$ 2.1	–
CIN (Bodnar et al., 2021a)	92.7 $\pm$ 6.1	68.2 $\pm$ 5.6	77.0 $\pm$ 4.3	83.6 $\pm$ 1.4	84.0 $\pm$ 1.6
<b>SUBGRAPH GNNs</b>					
DROPEdge (Rong et al., 2019)	91.0 $\pm$ 5.7	64.5 $\pm$ 2.6	73.5 $\pm$ 4.5	82.0 $\pm$ 2.6	82.2 $\pm$ 1.4
GRAPHCONV + ID-GNN (You et al., 2021)	89.4 $\pm$ 4.1	65.4 $\pm$ 7.1	71.9 $\pm$ 4.6	83.4 $\pm$ 2.4	82.9 $\pm$ 1.2
DS-GNN (GIN) (EGO+) (Bevilacqua et al., 2022)	91.0 $\pm$ 4.8	68.7 $\pm$ 7.0	76.7 $\pm$ 4.4	82.0 $\pm$ 1.4	80.3 $\pm$ 0.9
DSS-GNN (GIN) (EGO+) (Bevilacqua et al., 2022)	91.1 $\pm$ 7.0	69.2 $\pm$ 6.5	75.9 $\pm$ 4.3	83.7 $\pm$ 1.8	82.8 $\pm$ 1.2
GNN-AK+ (Zhao et al., 2022)	91.3 $\pm$ 7.0	67.8 $\pm$ 8.8	77.1 $\pm$ 5.7	85.0 $\pm$ 2.0	–
SUN (GIN) (EGO+) (Frasca et al., 2022)	92.1 $\pm$ 5.8	67.6 $\pm$ 5.5	76.1 $\pm$ 5.1	84.2 $\pm$ 1.5	83.1 $\pm$ 1.0
<b>NATURAL BASELINES</b>					
GIN + BatchNorm + RNF-PE (Sato et al., 2021)	90.8 $\pm$ 4.8	64.4 $\pm$ 6.7	74.1 $\pm$ 2.6	82.1 $\pm$ 1.5	81.3 $\pm$ 1.1
GIN + RNF-NORM	88.9 $\pm$ 5.1	67.1 $\pm$ 4.3	76.4 $\pm$ 4.8	81.8 $\pm$ 2.2	81.9 $\pm$ 2.5
<b>STANDARD NORMALIZATION LAYERS</b>					
GIN + BatchNorm (Xu et al., 2019)	89.4 $\pm$ 5.6	64.6 $\pm$ 7.0	76.2 $\pm$ 2.8	82.7 $\pm$ 1.7	82.2 $\pm$ 1.6
GIN + InstanceNorm (Ulyanov et al., 2016)	90.5 $\pm$ 7.8	64.7 $\pm$ 5.9	76.5 $\pm$ 3.9	81.2 $\pm$ 1.8	81.8 $\pm$ 1.6
GIN + LayerNorm-node (Ba et al., 2016)	90.1 $\pm$ 5.9	65.3 $\pm$ 4.7	76.2 $\pm$ 3.0	81.9 $\pm$ 1.5	82.0 $\pm$ 2.1
GIN + Layernorm-graph (Ba et al., 2016)	90.4 $\pm$ 6.1	66.4 $\pm$ 6.5	76.1 $\pm$ 4.9	82.0 $\pm$ 1.6	81.5 $\pm$ 1.3
GIN + Identity	87.9 $\pm$ 7.8	63.1 $\pm$ 7.2	75.8 $\pm$ 6.3	81.3 $\pm$ 2.1	80.6 $\pm$ 1.7
<b>GRAPH NORMALIZATION LAYERS</b>					
GIN + PairNorm (Zhao & Akoglu, 2020)	87.8 $\pm$ 7.1	67.1 $\pm$ 6.3	76.7 $\pm$ 4.8	75.8 $\pm$ 2.1	75.3 $\pm$ 1.4
GIN + MeanSubtractionNorm (Yang et al., 2020)	90.1 $\pm$ 5.4	68.0 $\pm$ 5.9	76.4 $\pm$ 4.6	79.2 $\pm$ 1.2	79.0 $\pm$ 1.1
GIN + DiffGroupNorm (Zhou et al., 2020)	87.8 $\pm$ 7.6	67.4 $\pm$ 6.8	76.9 $\pm$ 4.3	77.2 $\pm$ 2.6	77.1 $\pm$ 1.9
GIN + NodeNorm (Zhou et al., 2021)	88.3 $\pm$ 7.0	65.1 $\pm$ 8.3	74.5 $\pm$ 4.6	81.2 $\pm$ 1.4	79.4 $\pm$ 1.0
GIN + GraphNorm (Cai et al., 2021)	91.6 $\pm$ 6.5	64.9 $\pm$ 7.5	77.4 $\pm$ 4.9	81.4 $\pm$ 2.4	82.4 $\pm$ 1.7
GIN + GraphSizeNorm (Dwivedi et al., 2023)	88.2 $\pm$ 6.3	68.0 $\pm$ 8.1	77.0 $\pm$ 5.0	79.8 $\pm$ 1.5	80.1 $\pm$ 1.8
GIN + SuperNorm (Chen et al., 2023)	89.3 $\pm$ 5.6	64.7 $\pm$ 3.9	76.1 $\pm$ 4.7	83.0 $\pm$ 1.5	82.8 $\pm$ 1.7
GIN + GRANOLA-NO-RNF	89.7 $\pm$ 5.4	65.8 $\pm$ 5.7	76.6 $\pm$ 2.5	83.1 $\pm$ 1.2	83.0 $\pm$ 1.5
GIN + GRANOLA-MS	92.1 $\pm$ 4.8	69.8 $\pm$ 4.7	77.3 $\pm$ 3.5	84.3 $\pm$ 1.5	83.5 $\pm$ 1.8
GIN + GRANOLA	92.2 $\pm$ 4.6	69.9 $\pm$ 4.5	77.5 $\pm$ 3.7	84.0 $\pm$ 1.7	83.7 $\pm$ 1.6